TAMPEREEN TEKNILLINEN YLIOPISTO
TAMPERE UNIVERSITY OF TECHNOLOGY

Leo Janka

Thermally Sprayed Cr_3C_2-NiCr Coatings — Improving the Abrasion Resistance

Julkaisu 1605 • Publication 1605

Tampere 2018

Tampereen teknillinen yliopisto. Julkaisu 1605
Tampere University of Technology. Publication 1605

Leo Janka

Thermally Sprayed Cr_3C_2-NiCr Coatings — Improving the Abrasion Resistance

Thesis for the degree of Doctor of Science in Technology to be presented with due permission for public examination and criticism in Konetalo Building, Auditorium K1702, at Tampere University of Technology, on the 30th of November 2018, at 12 noon.

Tampereen teknillinen yliopisto - Tampere University of Technology
Tampere 2018

Doctoral candidate: Leo Janka
Laboratory of Materials Science
Faculty of Engineering Sciences
Tampere University of Technology
Finland

Supervisor: Professor Petri Vuoristo
Laboratory of Materials Science
Faculty of Engineering Sciences
Tampere University of Technology
Finland

Pre-examiners: Dr. Steve Matthews
Department of Chemical and Materials Engineering
The University of Auckland
New Zealand

Professor Michael Gasik
School of Chemical Engineering
Aalto University
Finland

Opponents: Dr. Steve Matthews
Department of Chemical and Materials Engineering
The University of Auckland
New Zealand

Dr. Helena Ronkainen
Teknologian tutkimuskeskus VTT Oy
Finland

ISBN 978-952-15-4271-8 (printed)
ISBN 978-952-15-4292-3 (PDF)
ISSN 1459-2045

Abstract

There are many industrial applications in which the surfaces of components are exposed to abrasive wear. Protecting such surfaces against harsh abrasive conditions sets high technical requirements for the materials; typically these materials must combine extreme hardness with adequate toughness. These requirements can usually be satisfied with alloys that consist of hard carbides in the ductile metal matrix, e.g. liquid-phase sintered bulk hardmetals. Large components can often be protected against wear by applying a coating to their surface. The processing of hardmetals into a dense wear-resistant surface layer is achieved solely by thermal spraying technology. In thermal spraying, the hardmetal particles are heated and projected towards the component's surface by high-pressure combustion. Nowadays for most industrial applications, this thermal spraying is done with a High Velocity Oxy-Fuel (HVOF) torch or, more recently, a High Velocity Air-Fuel (HVAF) torch.

Even though tungsten carbide (WC) based hardmetals, e.g. WC-Co and WC-CoCr, serve for the vast majority of abrasion resistant applications, these compositions have technical restrictions. These limitations include rapid oxidation above 500 °C and an incommensurate coefficient of thermal expansion with steels. Nevertheless, oxidation-resistant compositions that consist of up to 80 wt.% of chromium carbides in a nickel-chromium binder, commercially designed as Cr_3C_2-NiCr, are regularly utilized at high service temperatures. The major disadvantage of Cr_3C_2-NiCr is its inferior abrasion resistance when compared against WC-Co.

This work focuses on the characteristics of the Cr_3C_2-NiCr composition that influence its abrasion resistance at room temperature and above. A unique high-stress abrasion testing procedure for thermally sprayed coatings was established, wherein the sample was heated-up to the testing temperature by induction heating. Moreover, the coated samples underwent various heat-treatments, aimed at simulating high-temperature service.

The commercially available Cr_3C_2-NiCr coatings under study were varied by selecting different feedstock powders and spray technologies. However, there were only minor variations in their wear resistance after long heat-treatments. This was attributed to the dissolution of the carbides during spraying and the re-precipitation of the excess C and Cr as chromium carbides during the subsequent heat-treatment. The prolonged heat-treatment resulted in coarse carbides with a high degree of coalescence and thus equalized the variations in the as-sprayed microstructures.

In order to provide enhanced abrasion resistance at room and elevated temperatures, novel compositions were developed with only 10 wt.% of WC. Both experimental compositions, designated as $70Cr_3C_2$-10WC-20Ni and $80Cr_3C_2$-10WC-10Ni, demonstrated attractive abrasion properties in their as-sprayed state and after heat-treatment. The technical performance of the experimental coatings was attributed to the role of dissolved W as a substitutional solid solution strengthener. Moreover, the high carbide content in $80Cr_3C_2$-10WC-10Ni was considered essential to provide abrasion resistance at high temperatures.

Another major challenge in thermally sprayed coating is the spraying-induced dissolution of the carbides. The dissolved carbides supersaturate the binder of the as-sprayed coating with residual carbide elements, and thus make it brittle. Here, laser post-treatment was used to re-precipitate the residual carbide-forming elements from the brittle as-sprayed binder. This improved the room temperature abrasion resistance of the commercially available $75Cr_3C_2$-25NiCr and $45Cr_3C_2$-37WC-18NiCrCo coatings. In $75Cr_3C_2$-25NiCr the most promising improvement to its abrasion resistance was achieved when relatively low laser fluences were applied, which precipitated small nano-sized particles in the binder. In $45Cr_3C_2$-37WC-18NiCrCo, however, relatively high laser fluences had to be used. This resulted in the formation of hard and wear-resistant $(Cr,W)_2C$ grains.

Preface

The vast majority of this work was carried out at AC2T research GmbH (Wiener Neustadt, Austria). In addition, part of the experimental research was performed at the Laboratory of Material Science at Tampere University of Technology (Tampere, Finland). The research was funded by the Austrian Research Promotion Agency (FFG) under the project no. 839126 and by the Austrian COMET K2 Programme (Project XTribology, no. 849109). In addition, this work was also supported by the K.F. and Maria Dunderberg foundation.
I would like to thank my former co-workers at AC2T research GmbH for their assistance. Most notably Dipl.-Phys. Jonas Norpoth, Dipl.-Ing. Christian Katsich, and Dr. Manel Rodriguez Ripoll, all of whom supported me throughout the whole project. The contribution of Mr. Norpoth was especially important during the experimental research and later during the publication stage of this work. Furthermore, Dr. Reinhard Polak and Dr. Andreas Pauschitz provided a fruitful environment for the scientific work.
The topic of this work was partially introduced to me by Dr. Lutz-Michael Berger. Throughout my research, Dr. Berger's broad understanding about the history of hardmetal coatings and his fresh ideas about the Cr_3C_2-WC system were enormously helpful. Most of all, I am grateful to my supervisor, Prof. Petri Vuoristo, for his guidance and comments. Due to various logistical challenges, Prof. Vuoristo had to contribute extra effort to supervise my work, which demonstrated his character both as an educator and as a scientist. The staff at TUT were also extremely helpful in supporting my research and offering new ideas. In particular, M.Sc. Ville Matikainen was always willing to discuss the challenges I faced during this work and to help me with the experimental studies.
During my studies, I have been fortunate to have the support and encouragement of my whole family. In particular, my father always showed an interest in my work and devoted time to discussing the challenges I faced. In addition, my sister Marika greatly encouraged and advised me along the way.

Contents

Abstract **i**

Preface **iii**

Abbreviation **vii**

List of Publications **ix**

1 Introduction **1**
1.1 Background of the Research 2
1.2 Aim of the Work 3
1.3 Research Questions 4
1.4 Author's Contribution 5

2 High Velocity Thermal Spraying **7**
2.1 High Velocity Oxygen and Air-Fuel Processes 8
2.2 Deposition of the Coatings by HVOF 9

3 Cr_3C_2-Based Hardmetal Coatings **11**
3.1 Interstitial Carbides 11
3.2 Cr_3C_2-Based Coatings 13

4 Abrasive Wear **19**
4.1 Classification of Abrasion 19
4.2 Abrasion at High Temperatures 20
4.3 Abrasion of Thermally Sprayed Cr_3C_2-NiCr 21

5 Materials and Methods **23**
5.1 Feedstock Powders and the Deposition of the Coatings 23
5.2 Post-Treatments 24
5.3 Material Characterization 25
5.4 Wear Studies 26

6 Results and Discussion **27**
6.1 Characteristics of the Cr_3C_2-NiCr Coatings 27
6.2 Characteristics of the Laser Post-Treated Cr_3C_2-NiCr Coatings 35
6.3 Characteristics of the Cr_3C_2-WC-Ni Coatings 38
6.4 Characteristics of the Laser Post-Treated Cr_3C_2-WC-Ni Coatings 44

7 Conclusions **49**

7.1 Scientific Contribution 49
7.2 Suggestions for the Future Work 53

Bibliography **55**

Publications **67**

Abbreviation

a&s	Agglomerated and sintered
at.%	Atomic percent
BSE	Back-scattered electron
C	Carbon
Cr	Chromium
CTE	Coefficient of thermal expansion
DE	Deposition efficiency
EDX	Energy dispersive X-ray spectroscopy
FIB	Focused ion beam
HVAF	High velocity air-fuel
HVOF	High velocity oxy-fuel
HV_{load}	Vickers hardness value and load in kilograms
Ni	Nickel
SE	Secondary electron
SEM	Scanning electron microscopy
XRD	X-ray diffraction
Cr_3C_2	Orthorhombic chromium carbide
vol.%	Volume percent
W	Tungsten
WC	Hexagonal tungsten monocarbide
W_2C	Hexagonal tungsten hemicarbide
wt.%	Weight percent

List of Publications

I L. Janka, J. Norpoth, R. Trache, S. Thiele, and L.-M.Berger, "HVOF- and HVAF-Sprayed Cr_3C_2-NiCr Coatings Deposited from Feedstock Powders of Spherical Morphology: Microstructure Formation and High-Stress Abrasive Wear Resistance Up to 800 °C," *Journal of Thermal Spray Technology*, vol 98, No. 7 pp. 1720 – 1731, Oct. 2017.

II L. Janka, J. Norpoth, R. Trache, and L.-M. Berger, "Influence of heat treatment on the abrasive wear resistance of a Cr_3C_2-NiCr coating deposited by an ethene-fuelled HVOF spray process," *Surface & Coatings Technology*, vol 291, pp. 444 – 451, Apr. 2016.

III L. Janka, J. Norpoth, S. Eicher, M. Rodríguez Ripoll, and P. Vuoristo, "Improving the toughness of thermally sprayed Cr_3C_2-NiCr hardmetal coatings by laser post-treatment," *Materials and Design*, vol 98, pp. 135 – 142, May 2016.

IV L. Janka, L.-M. Berger, J. Norpoth, C. Tomastik, V. Matikainen, and P. Vuoristo, "Improving the high temperature abrasion resistance of thermally sprayed Cr_3C_2-NiCr coatings by WC addition," *Surface & Coatings Technology*, vol 337, pp. 296 – 305, March 2018.

V L. Janka, J. Norpoth, C. Tomastik, V. Matikainen, and P. Vuoristo, "Laser-induced precipitation of $(W_{1-x}Cr_x)_2C$: Mixed carbide phase for improved wear resistance of thermally sprayed hardmetal coatings," *Surface & Coatings Technology*, vol 337, pp. 177 – 185, March 2018.

1 Introduction

In various industrial applications, the surface of a component is exposed to mechanical degradation, i.e. wear. Especially abrasive wear, in which hard particles move along the surface and cause plastic deformation or removal of material, has a significant impact on the maintenance costs of various processing equipment. In an average industrial economy, the monetary losses arising from abrasive wear are estimated to be in the region of 1-4% of gross domestic product [1].
Even though the resistance against wear is not regarded as a material property, materials that consist of high hardness together with sufficient impact toughness are typically considered appropriate for wear protective applications [2]. In the 1920s, the increasing industrial demand for wear-resistant materials resulted in the development of cemented carbide [3]. In principle, cemented carbide is a binary-phase material, wherein hard tungsten carbide (WC) particles in a ductile cobalt matrix form a composite with high hardness and sufficient impact toughness [4, 5]. Over the following decades, its composition was constantly improved [4]. One of these early improvements involved alloying small amounts of chromium carbide (Cr_3C_2) into WC-Co to inhibit grain growth. This practice yielded cemented carbide grades with fine-grained WC. Later, compositions with alternative carbides and binders were also studied. For example, a composition with Cr_3C_2 grains in a nickel binder was developed for applications deployed at high-temperatures or in corrosive environments [6].
Because the price of the cemented carbide was high [1], likely already in 1930s technological means were sought after to deposit a thin cemented carbide layer onto a steel substrate. The 1940s saw the first reported trials for producing a cemented carbide coating by flame spraying [7]. However, the first commercially viable process was not achieved until the 1950s, by Union Carbide Corp., who developed detonation spraying [8]. In detonation spraying, the feedstock powder is heated and accelerated to supersonic velocities by cyclic-combustion. This thermal spraying process results in a dense, mechanically-adhered cemented carbide layer [9]. Later, this cyclic-combustion supersonic thermal spraying evolved into continuous-combustion thermal spraying, namely the high velocity oxy-fuel (HVOF) and high velocity air-fuel (HVAF) technologies [10]. Both of these methods, HVOF and HVAF, are still regarded as the state-of-the-art spraying processes for cemented carbide coatings today.
Strictly speaking, the terms hardmetal or cemented carbide are used in bulk materials to denote WC-Co compositions. In thermal spraying, however, the term hardmetal is used in a broader sense to describe compositions that contain carbides in a metallic binder. Thus, hardmetal coatings could mean e.g. WC-Co, Cr_3C_2-NiCr, Cr_3C_2-WC-Ni or even (Ti,Mo)(C,N)-Ni compositions. Of these, however, it is the WC-based compositions that have the major share of the feedstock market.

[1] In early 1930s cemented carbide was more precious than gold [4]

1.1 Background of the Research

Even though WC-based hardmetals (e.g. WC-12Co and WC-10Co-4Cr) serve the vast majority of thermally-sprayed wear resistant applications, these compositions have technical limitations. One major drawback is their limited service temperature [11]. This stems from the low coefficient of thermal expansion (CTE) of WC-Co, which is incommensurate with the CTE of the steel substrate [2]. In addition to this, rapid isothermal oxidation occurs at above 550 °C [11, 14]. Thus, internal stresses can occur inside the coating during high-temperature service which can result in cracking of the coating. Cracking combined with the formation of a thick oxide scale makes the cemented carbide layer prone to delamination above 550 °C. Another prominent challenge for WC-based cemented carbide is the intense price fluctuation of tungsten, and its geographically limited availability [15, 16]. As a consequence, the European Commission has classified tungsten as a critical raw material, for which substitutes must be found in the future [17].
In an effort to address the above-mentioned technical restrictions of cemented carbide coatings, in the 1960s Union Carbide Corp. patented and commercialized two coating compositions containing Cr_3C_2: binary-carbide 70WC-24Cr_3C_2-6Ni [18] and plain chromium carbide 75Cr_3C_2-25NiCr [19]. Both of these early patent documents describe mechanical blends of coarse carbides and nickel particles. However, nowadays the feedstock powders for HVOF and HVAF spraying are mainly produced by agglomerating and sintering (a&s) and thus contain finer carbides than the early feedstock powders. The first composition, 70WC-24Cr_3C_2-6Ni, has better resistance to corrosion and high-temperature oxidation than WC-Co, while still maintaining high wear resistance [20 – 22]. The plain chromium carbide composition, 75Cr_3C_2-25NiCr, has even better corrosion and oxidation resistance [11]. In addition, the CTE of Cr_3C_2 is close to that of ferritic steel [12, 13], which means that 75Cr_3C_2-25NiCr coating is not nearly as susceptible to cracking at high-temperatures as WC-containing coatings. Its wear resistance, however, is significantly inferior to WC-Co [23]. 75Cr_3C_2-25NiCr compositions sprayed by HVOF and HVAF are today widely used in the manufacturing and energy industries in service temperatures of up to 900 °C. Nevertheless, there is a pressing industrial demand to improve its wear resistance still further, without sacrificing any of its superior high-temperature properties.
In the 2000s, interest in novel binary carbide coatings soared. In 2005, Metco introduced a WOKA 7500 series (Sulzer Metco, Switzerland) a&s powder, with a designation of 45Cr_3C_2-37WC-18Ni [24]. Recently, the corresponding Amperit 543 series (H.C. Stark, Germany) a&s feedstock powder with a designation of 42Cr_3C_2-42WC-16Ni has also appeared as a commercial feedstock powder. While Koffskey's early patent describes WC-rich compositions [18], these recent compositions, WOKA 7500 series and Amperit 543 series, show close to an equal Cr_3C_2/WC-ratio in wt.%. Although the manufacturers of these feedstock powders have not given any clear reasons for the reduced WC content, historically the development of binary carbide compositions for thermal spraying appears to be the outcome of empirical research, rather than the result of systematic studies.
During the thermal spraying of carbide-containing coatings, the heat dissolves the carbides into a binder, and this is followed by the rapid quenching of the feedstock particles. Hence, the deposition process leaves the metallic binder of an as-sprayed coating in a metastable state. Given the supersaturated and even amorphous nature of the binder, the as-sprayed coating is often prone to brittle fracture [25]. The properties of as-sprayed coatings can be enhanced by post heat-treatment [26]. The heat-treatment enables the metastable and brittle binder to transform to equilibrium phases through the precipitation of the

[2] the CTE of ferritic steel is $11 - 12 \times 10^{-6} K^{-1}$ [12] and the CTE of WC is $6.9 \times 10^{-6} K^{-1}$ [13]

carbides, which yields increased carbide content and ductile binder [25, 27–30]. The conventional heat-treatment of coatings in a furnace poses various challenges though, such as delamination of the coating and residual warping in thin substrates. Moreover, the furnace has to be big enough for the coated component, which often means that post heat-treatment is only possible with relatively small components. These problems can be avoided with laser post-treatment, wherein the laser-induced heat input is confined solely to the coating. Due to the rapid development of high-power diode lasers and optical systems, laser post-treatment is a potentially viable process, not only for small components, but also for larger ones [31]. Laser treatment trials on thermally sprayed hardmetal coatings have been reported in refs. [32–41]. In all of these studies, the laser fluence and irradiance levels were high, which resulted in the remelting of the binder phase[3]. The remelting treatment improves the resistance to erosive [34, 37] and dry-sliding wear [32]. However, there have been reports of severe cracking of laser remelted surfaces [33].

1.2 Aim of the Work

Even though thermally sprayed Cr_3C_2-NiCr coatings have been widely studied over the last 50 years, some important aspects have been overlooked. One of these is their abrasion resistance at high temperatures. As there is no ASTM wear testing standard for the high-temperature abrasion resistance of thermally sprayed coatings, a testing procedure which had previously been used for high-temperature abrasion testing of hardfacings [42, 43] was used in this work. Briefly put, this procedure is a high-temperature modification of the ASTM B611 standard, wherein the sample is heated to the testing temperature by induction heating while a rotating steel wheel induces wear loss by pressing and sliding dry abrasive particles on the surface of the sample.
The first goal in this work is to understand the microstructural features that influence the abrasion resistance of HVOF and HVAF sprayed 75Cr_3C_2-25NiCr coatings. It is known that various parameters, such as the manufacturing route of the feedstock powder, the spray process, and heat-treatment have a major impact on the microstructure of the coating [11, 30, 44–46]. However, these microstructural features have yet to be linked to high-stress abrasion resistance, either at room temperature or at elevated temperatures.
The second goal of this work is to study the effect of adding WC to Cr_3C_2-based coatings. Therefore, experimental spray feedstock powders with 10 wt.% of WC were manufactured, deposited and characterized. Fig. 1.1 presents the Cr_3C_2/WC-ratio of both the commercially available and the experimental binary carbide compositions. The compositions studied here are shown in the light grey boxes. As can be seen in fig. 1.1, the Cr_3C_2-rich side on the left has no currently-available WC containing commercial feedstock powders. In fact, the lack of both commercially available coatings and academic studies on the Cr_3C_2-rich binary carbide compositions was one of the main motivations for this work. The experimental 70Cr_3C_2-10WC-20Ni and 80Cr_3C_2-10WC-10Ni coatings were developed for the following reasons. Firstly, the metallurgical interactions between WC and Cr_3C_2 in Cr_3C_2-based compositions have not been studied systematically. Secondly, if we can reduce the WC content in the coatings we can preserve our dwindling strategic tungsten resources. Thus, in this study the room-temperature and high-temperature abrasion resistance of the experimental coatings was benchmarked against the commercially available 75Cr_3C_2-25NiCr and 45Cr_3C_2-37WC-18NiCo coatings.
In previous studies it has been shown that the microstructure of 75Cr_3C_2-25NiCr is highly

[3] sometimes this post-treatment is called laser glazing

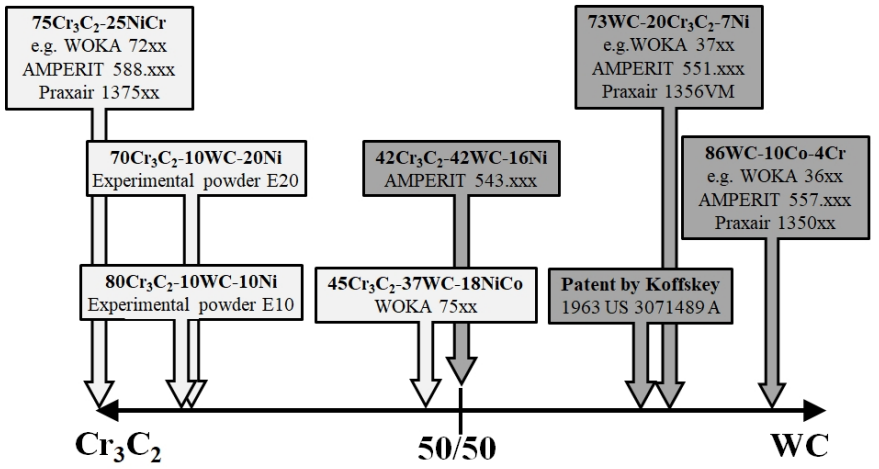

Figure 1.1: Commercially available and the experimental WC-Cr_3C_2 binary carbide compositions classified by their Cr_3C_2/WC-ratio. The bright gray-scale boxes designate the compositions studied in this work.

susceptible to heat-treatment [25, 26, 30]. This characteristic was utilized here by tailoring the microstructure and the abrasion resistance of the coatings by laser heating. Until now, laser post-treatment procedures have been used to remelt the coating. However, the rapid solidification of hardmetals after laser remelting often leads to cracking of the coating. In this work, therefore, the laser heat was used solely to precipitate the residual carbide-forming elements as carbides, while the coating remained in a solid state throughout this post-treatment procedure. The solid-state treatment by laser was performed on HVOF sprayed 75Cr_3C_2-25NiCr and 45Cr_3C_2-37WC-18NiCr coatings.
This work is arranged as a compilation study. Chapters 2-4 present the theoretical background of the work. Chapter 5 describes the methodology of the study. Chapter 6 demonstrates the most important findings of the work. Chapter 7 presents the conclusions. In addition, the scientific findings are presented in detail in the five original publications appended to this thesis.

1.3 Research Questions

This work aims to answer the following research questions. These question are divided into four sections.

I Cr_3C_2-NiCr coatings

1. What roles do the feedstock powder consolidation method (sintering vs. plasma-densification) and the spray process (gas-fueled HVOF, liquid-fueled HVOF, and HVAF) method play in the microstructure of the 75Cr_3C_2-25NiCr coating?

2. How does the microstructure of the coating influence the abrasion protection capacity of thermally sprayed Cr_3C_2-NiCr coatings at room and elevated temperatures?

II Laser treated Cr_3C_2-NiCr coatings

3. Can the high-stress abrasion resistance of Cr_3C_2-NiCr coating be improved by laser-induced nanosized chromium carbide precipitation?

III WC alloyed Cr_3C_2-Ni

4. How do the interactions between the WC and Cr_3C_2 grains influence the microstructure and mechanical properties in 10 wt.% WC-alloyed Cr_3C_2 based coatings?
5. What is the contribution of the 10 wt.% WC addition to the abrasion resistance of the Cr_3C_2-based coatings?
6. What is the significance of the metallic binder content in the abrasion resistance of the WC-alloyed Cr_3C_2-rich coatings?

IV Laser treated Cr_3C_2-WC-Ni coatings

7. Is it possible to precipitate the $(W_{1-x}Cr_x)_2C$ phase in the binder of the as-sprayed binary carbide Cr_3C_2-WC-Ni coatings by laser post-treatment without remelting the coating?
8. Do Cr-rich $(W_{1-x}Cr_x)_2C$ precipitates improve the abrasion resistance of the coating?

These research questions have now been addressed in publications I-V. Table 1.1 lists the corresponding publication and chapters in this dissertation wherein the above research questions are discussed.

Table 1.1: Research questions

Publications	Papers I & II	Paper III	Paper IV	Paper V
Chapter	6.1	6.2	6.3	6.4
Theme	Commercial Cr_3C_2-NiCr coatings	Laser treated Cr_3C_2-NiCr	WC alloyed Cr_3C_2-Ni	Laser treated Cr_3C_2-WC-Ni
Research questions	1 & 2	3	4-6	7 & 8

1.4 Author's Contribution

Publication 1:
The coatings were deposited mainly by the industrial partners and the powder characterization was performed at Fraunhofer IKTS. The author refined and planned the testing procedure, and later conducted the coating characterization and wear testing. Furthermore, the author gathered the data for the publication, wrote the first draft, and later revised it with the co-authors.

Publication 2:
The coatings were deposited by an industrial partner. The author planned the testing procedure, and later conducted the coating characterization and wear testing. The author

wrote the first draft of the manuscript and later revised it with the co-authors.

Publication 3:
The coatings were deposited by Fraunhofer IKTS and the subsequent post-treatments were planned and executed by the author. Moreover, the author organized and supervised the metallography and wear testing. Furthermore, the author wrote the first draft of the manuscript and revised it with the co-authors.

Publication 4:
Feedstock preparation and powder characterization along with the deposition was performed at Fraunhofer IKTS. The author conducted the coating characterization and wear testing. However, the nanohardness tests were performed by Dr. Christian Tomastik. The author planned the publication and wrote the first draft of the manuscript and later revised it with the co-authors.

Publication 5:
The coatings were deposited by Frauhofer IKTS and the post-treatments were planned and executed by the author. The author executed the coating characterization and wear testing. Nanohardness was probed by Dr. Christian Tomastik. The author wrote the first draft of the manuscript and later revised it with the co-authors.

2 High Velocity Thermal Spraying

The history of thermal spray technology originated from Max Ulrich Schoop's invention [47]. The first *Scoop-pistol* was essentially a flame spraying torch, especially used to spray coatings for corrosion protection. Nowadays, thermal spraying comprises a variety of processes in which the coatings are deposited by heating the feedstock material and accelerating the droplets or softened feedstock particles onto the substrate in a gas stream [10, 48]. These processes can be roughly classified by the sources of the heating energy, which include electric arc (e.g Arc or Plasma spraying), kinetic energy (e.g Cold Gas Dynamic spraying), or combustion (e.g Flame or High Velocity Oxy-Fuel spraying) [10, 48, 49]. Fig. 2.1 gives a rough comparison of the thermal spray processes based on the feedstock particle temperature and velocity during deposition of the coating.
As the goal in hardmetal spraying is to achieve a dense coating with minimal decomposition of the hard carbides, the hardmetal feedstock powder requires a high particle velocity together with an intermediate particle temperature. The particle temperature should be lower than the decomposition temperature of the carbides and yet result in partial melting of the metallic binder and only minimal dissolution of the carbides. As presented in Fig. 2.1 these requirements are best filled by High Velocity Oxy-Fuel (HVOF) and High Velocity Air-Fuel (HVAF) torches. These spray technologies are discussed in detail below.

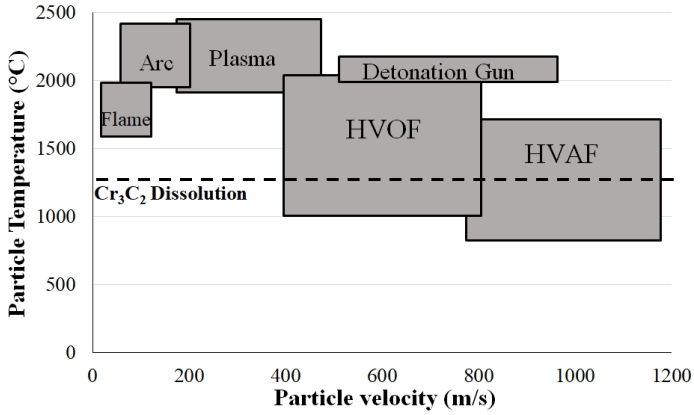

Figure 2.1: Rough comparison of the particle temperatures and velocities of various thermal spraying technologies. The lowest dissolution temperature of Cr_3C_2 is presented in the figure. Based on refs. [10, 48, 49].

2.1 High Velocity Oxygen and Air-Fuel Processes

The development of HVOF spraying by James A. Browning dates back to the late 1970s and early 1980s [50]. However, this technology can be seen as a development of cyclic-combustion detonation spraying [51]. In principle, HVOF is based on the continuous combustion of air and hydrocarbons or hydrogen in a combustion chamber, which is followed by the acceleration of the flow of the expanding gas in the nozzle [51, 52]. Browning's *Jet Kote* HVOF torch was introduced in 1982 and presented attractive technical properties at that time. However, the first-generation HVOF torches are now considered inferior to modern equipment in terms of spray economics and the technical performance of the coatings [53]. During the further development of HVOF in the 1980s and 1990s, the trend was towards higher jet velocity. This was largely achieved by higher pressure in the combustion chamber and *De Laval* convergent-divergent nozzle design [51, 54, 55]. Figure 2.2 shows a third generation kerosene-fueled *JP5000* HVOF torch, wherein the powder feedstock is fed radially into the nozzle. The combustion products yield a supersonic jet of gas that accelerates and heats the feedstock powder. The evolution

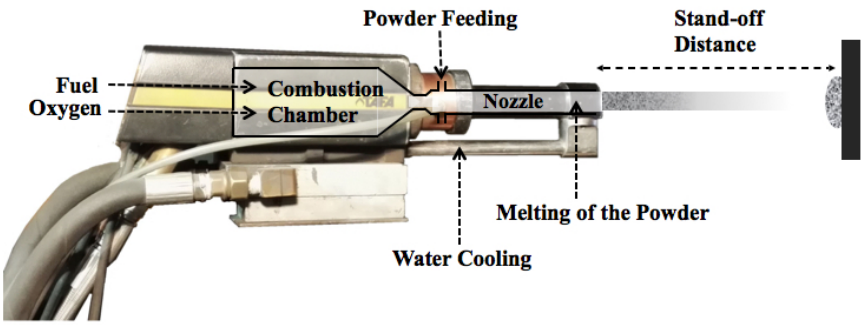

Figure 2.2: Third generation JP5000 liquid fuel HVOF torch with radial powder feeding.

of the HVOF-process resulted in denser coatings and improved spray economics because of the higher feedstock deposition rates. Besides the torch design, another important variable is the combustion fuel. Figure 2.3 summarizes the flame temperature of various fuels as a function of oxy-fuel ratio (λ), wherein value 1 represents stoichiometric combustion. Until recently, the HVOF process has been regarded as the state-of-the-art deposition process for hardmetals. However, lately the popularity of HVAF spraying has increased [22, 57–60]. The main idea behind HVAF was to decrease the particle temperatures and reduce the operating costs by using air instead of expensive oxygen [61]. However, given its poor deposition efficiency, HVAF was not considered to be an economically competitive technology to HVOF till the early 2000s [60, 62] when its further development led to stable combustion and axial powder injection [63]. The recent improvements in HVAF technology have been largely driven by Kermetico, Inc. (CA, USA) with their *AK* torches and Uniquecoat Technologies, LLC. (VA, USA) with the *M3* torch. The major difference between these two spray torches stems from the nozzle design; the M3 torch includes secondary air and fuel injection in the nozzle [64].

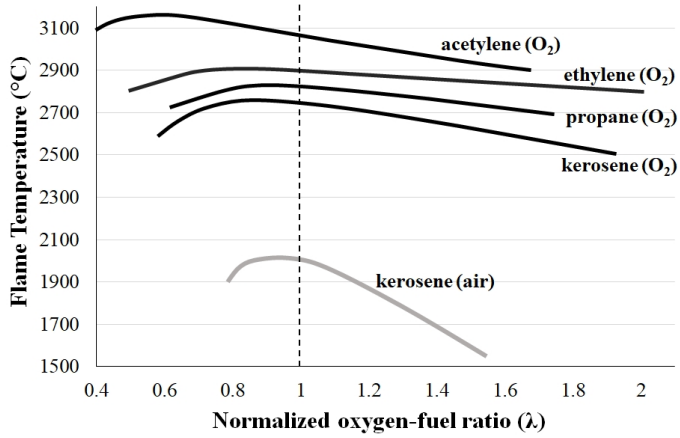

Figure 2.3: The influence of combustion fuel and flame stoichiometry on flame temperature. Reproduced from ref. [56].

2.2 Deposition of the Coatings by HVOF

A thermally sprayed coating is essentially formed from individual deformed particles (i.e. splats) and represent laminar microstructure [65]. Typical defects in the microstructure of the coating arise from the spraying process and include both porosity and oxide stringers in the splat boundaries [10, 66]. In HVOF spraying, the typical thickness of a layer is in the range of 10-40 μm [65]. Thus, several passes by the spray torch over the substrate are needed in order to build-up the coating (usually 100-500 μm thick).

2.2.1 In-flight behavior

From the moment the feedstock powder is fed into the hot gas stream of the spray torch, the powder particle undergoes rapid acceleration and heating. The acceleration of the particle is defined by the characteristics of the flame and the feedstock particle. The velocity and viscosity of the combustion gas combined with the particle size and density play the most pronounced role in the acceleration [65, 67]. Moreover, the particle temperature during flight is defined by the temperature of the gas stream, heat transfer from the gas to the particle, and the thermal properties of the feedstock particles [65]. While in-flight, the powder particles react with the atmosphere and can undergo various chemical changes, such as oxidation and decarburization. Obviously, the stoichiometry of the flame has a major bearing on the in-flight oxidation of the particles [66]. Moreover, the mixing of the surrounding air elevates the oxygen partial pressure in the tail flame of the HVOF torch [68]. Because of the oxidized particles, the microstructure of as-sprayed coating has oxide stringers between the splats [66]. However, not all the oxygen pick-up in thermal spray coating is due to in-flight oxidation. The surface is exposed to the oxidizing tail flame, while the torch traverses over the coating [68]. Thus, a higher number of passes by the spray torch further increases the oxygen content in the coating [69]. Decarburization is another important phenomenon that occurs during hardmetal deposition. It is attributed to a mechanism involving the dissolution of carbide in the liquid binder followed by oxidation of C at the surface of the particle

[70]. In WC-based compositions, this phenomenon is later characterized by the presence of tungsten hemicarbide (W_2C) in the deposited coating. The carbon loss can also be a result of selective rebounding of hard constituents of the feedstock granules, when coarse solid carbides predominantly rebound during the impact of the particle on the surface [45, 57, 69]. This selective carbide rebounding is increased by pronounced granule melting during spraying and coarse carbide size in the granules [45]. Matikainen et al. [57] suggested that selective carbide rebounding is dominant carbon loss mechanism when agglomerated and sintered (a&s) feedstock powder, with relatively coarse carbides and high intragranular porosity, was used in HVAF spraying. Therefore, plasma-densified feedstock powder, which consists of fine uniformly distributed carbides in dense and round granules, was considered beneficial in HVAF spraying [57].

2.2.2 Impact of the particles

As the accelerated molten or semi-molten particles reach the substrate they undergo both severe plastic deformation and rapid quenching. The flattening of the particle depends on both the substrate and the particle characteristics. The kinetic energy and the degree to which the particle has melted clearly have the most pronounced influence on this flattening (i.e. splat formation). Moreover, a harder substrate promotes the conversion of kinetic energy into heat and thus, more plastic deformation, which improves the flattening of the particle [71].
The rapid solidification of the particle leads to tensile residual stresses within the splat. However, owing to the high kinetic energy of the impacting particles in HVOF spraying, the subsequent layer of particles yields a shot peening effect in the previously deposited solidified layer of splats [72]. Therefore, the residual stresses inside HVOF-deposited coatings are usually compressive. Furthermore, the peening effect from the impacting particles also increases the density of the underlying layer. Because the molten or semi-molten particles cool rapidly upon reaching the substrate, the coating does not form a metallurgical bond with the substrate. The residual stresses of the coating, however, result in mechanical anchoring [10, 48, 65]. Therefore, prior to the deposition of the coatings, the substrate is prepared by grit blasting in order to roughen its surface enough for the mechanical anchoring to take place.
During the deposition of hardmetal feedstock, a delicate temperature balance is required. If the temperature is too low, the deposition efficiency of the powder is low because the metallic binder has not melted enough. On the other hand, if the temperature is too high, it promotes pronounced carbide dissolution, or even decomposition. The ideal temperature yields partial melting of the metallic binder and thus satisfactory splat formation upon impact without any significant loss of the carbide phase. In addition, high particle velocities are required in order to produce a dense coating with compressive residual stresses.

3 Cr_3C_2-Based Hardmetal Coatings

Refractory carbides are hard compounds with a high melting point [73]. In industry they are used widely in numerous applications, e.g as hard phases in wear resistant alloys, grinding wheels, and cutting tools. The production of hardmetals involves the utilization of large quantities of carbides; bulk hardmetal components typically consist of 80-95 wt.% of carbides [5]. The suitability of various refractory carbides to form composites with a metallic binder stems from the good wettability of solid carbide grains by liquid metal [74].

3.1 Interstitial Carbides

An important sub-category of refractory carbides is known as interstitial carbides. These are crystalline compounds, wherein the carbon occupies the interstices of the host metal lattice [73]. Even though interstitial carbides have been studied intensively in the past, the exact nature of the atomic bonding is still a rather controversial subject. Usually, the atomic bonding in interstitial carbides is described as a combination of ionic, covalent and metallic bonding [73, 74]. This partially explains why they often exhibit the physical properties of ceramics (e.g. high hardness and melting temperature) and the electric properties of metals (e.g. high thermal and electric conductivity) [73]. Table 3.1 presents the properties of the technically important transition Group VI chromium and tungsten carbides.

Table 3.1: Selected industrially relevant carbides and their properties [13, 75].

	WC	W_2C (β'')	Cr_3C_2	Cr_7C_3
Crystal system	Hexagonal	Hexagonal	Orthorhombic	Orthorhombic
Pearson symbol	$hP2$	$hP3$	$oP20$	$oP40$
Hardness (HV) [1]	2700	3000	2650	1336
Elastic modulus (GPa)	710	421	386	-
Density (g/cm^3)	15.63	17.34	6.68	6.99
CTE ($10^{-6}K^{-1}$)	6.9	3.84	10.3	11.7
Decomposition	Peritectic	$\beta'' \leftrightarrow \beta'$	Peritectic	Congruent
(°C)	2785	2100	1811	1766

[1] The grain orientation or load was not specified

3.1.1 Tungsten carbides

There are two carbide compounds in the W-C equilibrium diagram: WC and W_2C [76]. Hexagonal WC was first synthesized in the 1890s and later widely commercialized as a major phase in cemented carbides [77]. The mechanical properties of WC depend on the grain orientation. In the early work of Pons [78], indents placed on the prismatic $(10\bar{1}0)$ and basalt (0001) planes yielded Vickers hardness ($HV_{0.02}$) values of 1450 and 2500, respectively. The lower prismatic plane hardness can be explained by the plastic deformation induced by dislocation migration in WC [79], which is—again—a strong indication of the metallic properties in interstitial carbides.
The lower tungsten carbide, W_2C compound, has three polymorphic modifications: C6 hexagonal β'', orthorhombic β', and L´3 hexagonal β [76]. In thermally-sprayed coatings, W_2C is often a byproduct of spraying-induced carbon loss in the WC [70, 80]. In addition, fused tungsten carbide powders for hardfacings contain a mixture of WC and W_2C [81]. Despite its high hardness, W_2C is often considered detrimental due to its low ductility [82]. Even though there are no consistent comparisons of the plastic deformation and atomic bonding of β''-W_2C and WC, it is likely that the degree of metallic bonding varies in these carbides.
Despite the fact that WC remains hard in high temperatures [77, 83], the use of WC-containing alloys at such temperatures is restricted by the rapid oxidation of WC at above 500 °C [14, 84]. Another challenge is the low CTE of WC [13], which may lead to cracking and delamination of the thermally-sprayed WC-based coating at high temperatures [11].

3.1.2 Chromium carbides

The Cr-C equilibrium diagram presents three carbide compounds: orthorhombic Cr_3C_2, orthorhombic Cr_7C_3, and cubic $Cr_{23}C_6$ [85]. A decreased C content decreases the hardness; Mayr et al. [86] reported hardness values of 26.6 GPa for Cr_3C_2, 20.2-23-6 GPa for Cr_7C_3 and only 14.1 GPa for $Cr_{23}C_6$. Therefore, Cr_3C_2 is regarded as the most desirable chromium carbide phase in wear-resistant alloys. However, wear-resistance in Fe-Cr-C hardfacings [87] and high-chromium white cast irons [88] is provided by Cr_7C_3 carbide, which precipitates from the solid during slow cooling of the alloy.
The chemical resistance of Cr_3C_2 is far superior to WC. Therefore, WC is often replaced by Cr_3C_2 in alloys which will be subjected to high temperatures or chemically aggressive environments [11, 14, 84]. In addition, the CTE of Cr_3C_2 is close to the CTE of ferritic steel [12, 13], which further improves the service characteristics of Cr_3C_2-based coatings at high temperatures.

3.1.3 Mixed tungsten-chromium carbides

Mixed tungsten-chromium carbides were first reported by Westegren in 1933 [89]. Due to the importance of chromium carbide as an alloying element in WC-Co hardmetals [5], the interactions between WC and Cr_3C_2 were characterized in the 1960s by Stecher et al. [90] and Rudy et al. [91]. These two studies have some contradictions, however, e.g. the equilibrium diagram by Stecher et al. shows lower solubility of Cr in WC than that estimated by Rudy et al. Later a study by Brieseck et al. [92] defined the maximum solubility of Cr in WC as 1.5 at.%. The solubility of Cr in W_2C is significantly higher; W_2C can contain over 55 at.% of Cr [90, 91, 93]. Surprisingly, the impact of the Cr content on the mechanical properties of $(W_{1-x}Cr_x)_2C$ has not been systematically studied.
The solubility of W in Cr_3C_2, Cr_7C_3, and $Cr_{23}C_6$ was reported to be 8.8, 3.8, and

12.7 at.%, respectively [90]. The impact of W on the mechanical properties of chromium carbides is still largely uncharacterized. Yamamoto et al. [94] studied the hardness of W alloyed Cr_7C_3 at room and high temperatures. Interestingly, the W content of 1.4 at.% increased the hardness of the $(Cr,W)_7C_3$ grains markedly at 600 °C. However, at room temperature, the contribution of W alloying to carbide hardness was almost negligible.

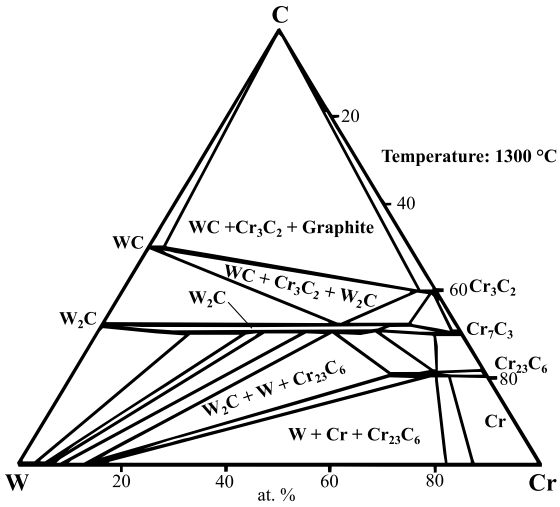

Figure 3.1: Isothermal section at 1300 °C of the W-Cr-C ternary equilibrium diagram by [91]. Reproduced from ref. [95].

3.2 Cr_3C_2-Based Coatings

Thermally sprayed hardmetal coatings based on Cr_3C_2 carbides are widely used as wear protective coatings at high temperatures and in corrosive environments. Especially in the heavy industrial sectors, such as metal processing, energy, and oil&gas, these coatings are deployed in various applications [96, 97]. As a consequence, nowadays Cr_3C_2-NiCr is the second most used hardmetal composition for thermal spraying. Here, the metallurgy of the Cr_3C_2-Ni system and the properties of the coatings are discussed.

3.2.1 Metallurgy of Cr_3C_2-NiCr

Fig. 3.3 presents the Ni-Cr-C ternary equilibrium diagram at 800 °C by Velikanova et al. [98]. The system contains three chromium carbides: Cr_3C_2, Cr_7C_3, and $Cr_{23}C_6$. In Cr_7C_3 and $Cr_{23}C_6$ the maximum solubility of Ni is 6 at.% and 5 at.%, respectively. In Cr_3C_2, the maximum Ni solubility is considerable lower, only 0.7 at.%. However, as Ni does not markedly change the lattice size in chromium carbides, its content in Cr_7C_3 grains is difficult to probe by X-ray diffraction [98]. The solubility of C into solid Ni is low; in a Ni-C binary system the C solubility at 800°C is only 0.5 at.% [99]. However, the Ni(Cr) solid solution shows higher C solubility than plain Ni. At 13.6 at.% of Cr in a Ni(Cr)-lattice the C solubility is approximately 2 at.% at 800 °C.
Fig. 3.3 shows the vertical Cr_3C_2-$Ni_{90}Cr_{10}$ section of the ternary Ni-Cr-C system. The Cr_3C_2 is a stable phase with Ni(Cr) below 1255 °C. This is a major benefit of a Ni(Cr)

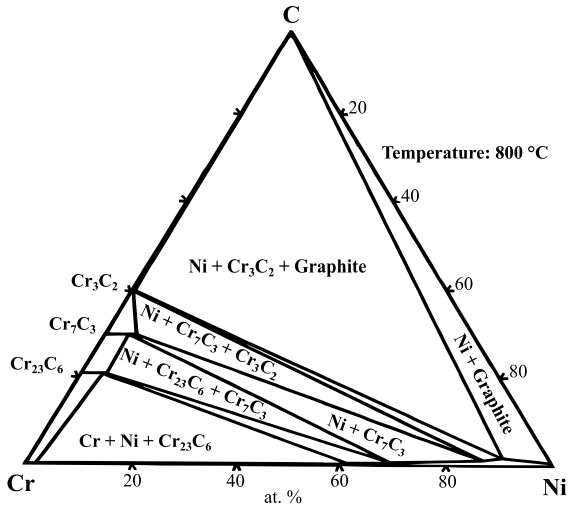

Figure 3.2: Isothermal section at 800°C of the Cr-Ni-C ternary equilibrium diagram. Reproduced from ref. [98].

solid solution over plain Ni. Because in the vertical Cr_3C_2-Ni section, presented by Velikanova et al. in ref. [98], a detrimental graphite phase coexists with the Cr_3C_2 and Ni below 1255 °C. Above 1255 °C in the vertical Cr_3C_2-$Ni_{90}Cr_{10}$ section, the Cr_3C_2 transforms into Cr_7C_3 and later dissolves into liquid nickel. This dissolution of Cr_3C_2 is a major challenge in thermally-sprayed Cr_3C_2-NiCr coatings. During thermal spraying, the temperature of the particles far exceeds the Ni(Cr) melting temperature and thus results in the dissolution of the Cr_3C_2. However, as the subsequent solidification of the semi-molten feedstock particles is rapid, the Cr_3C_2 does not have time to re-precipitate, i.e. the system does not reach equilibrium, leaving the binder supersaturated with Cr and C [25].

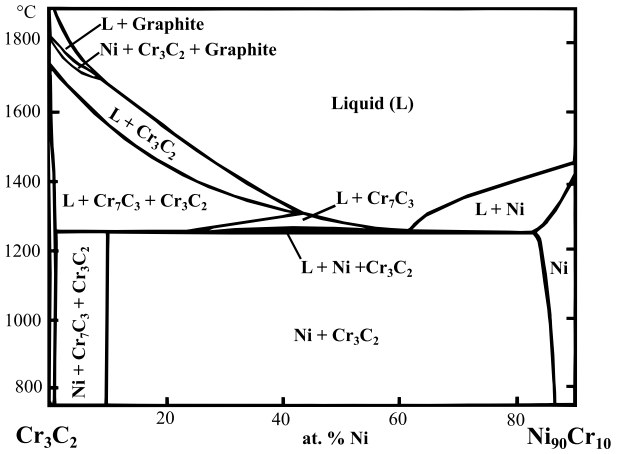

Figure 3.3: Vertical section from Cr-Ni-C ternary equilibrium diagram through Cr_3C_2-$Cr_{10}Ni_{90}$. Reproduced from ref. [98].

3.2.2 Thermally sprayed Cr_3C_2-NiCr

Cr_3C_2-Ni bulk cermets were reportedly already used in the 1950s to provide resistance against wear in high-temperature applications [6]. In the 1960s, Union Carbide Corp. patented Cr_3C_2-NiCr feedstock powder for thermal spraying [19]. This first patent comprised a mechanical blend of coarse Cr_3C_2, Ni, and Cr particles. Today, the modern spherical Cr_3C_2-NiCr feedstock powders for thermal spraying are based on spray-dried (agglomerated) granules [11]. After the spray-drying, both sintering and plasma-treatment can be used to consolidate the granules. Agglomerated and sintered (a&s) granules are characterized by their high intragranular porosity and the incomplete embedding of the carbides in the binder. In contrast, plasma-treated powders display a dense structure that consists of fine dendritic carbides, which is due to the melting and solidification of the powder during consolidation [11]. Fig. 3.4 presents the morphology of agglomerated and sintered (a) and agglomerated and plasma-densified (b) feedstock granules.

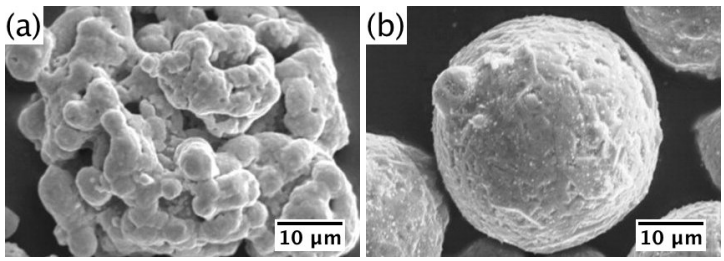

Figure 3.4: The morphology of agglomerated and sintered (a) and agglomerated and plasma-treated (b) Cr_3C_2-NiCr granules. Reproduced from ref. [100].

In the 1960s, the main deposition method for Cr_3C_2-NiCr coating was the detonation gun [19]. Due to the development of plasma spraying technology, later atmospheric plasma spraying also became an industrially relevant deposition method [101, 102]. Nowadays, HVOF spraying and, more recently, HVAF spraying have become established as the most frequently used spraying processes for Cr_3C_2-NiCr coatings [11]. As stated earlier, the dissolution of Cr_3C_2 into molten Ni already begins at 1255 °C [98]. Thus, reduced heat input into the feedstock granules during spraying, which is a characteristic feature in HVAF spraying, yields coatings with hindered carbide dissolution [57, 58].
In the as-sprayed state, the partially amorphous binder is supersaturated by residual carbide-forming elements, namely C and Cr. Therefore, heat-treatment, either during high-temperature service or as a tailored post-treatment procedure, alters significantly the microstructure of Cr_3C_2-NiCr. At elevated temperatures, the residual carbide-forming elements in the binder precipitate as chromium carbides [25, 27–30, 103]. This precipitation process already begins at 400 °C [25, 30]. The transition of the binder from partially amorphous and C-supersaturated solid-solution towards the crystalline NiCr increases the ductility, and thus improves the wear resistance of the coating at room temperature under erosive [25, 29] and sliding wear [26] conditions. Further heat-treatment of the coating yields a coarse Ostwald-ripened carbide skeleton and an essentially C-free binder [27–30]. The coarse carbide structure increases the hardness of the coating [28]. This microstructural evolution is illustrated in fig. 3.5, where the HVOF sprayed coating is presented in its as-sprayed state (a) and after heat-treatment at 900 °C for 2 days (b), 20 days (c) and 60 days (d).

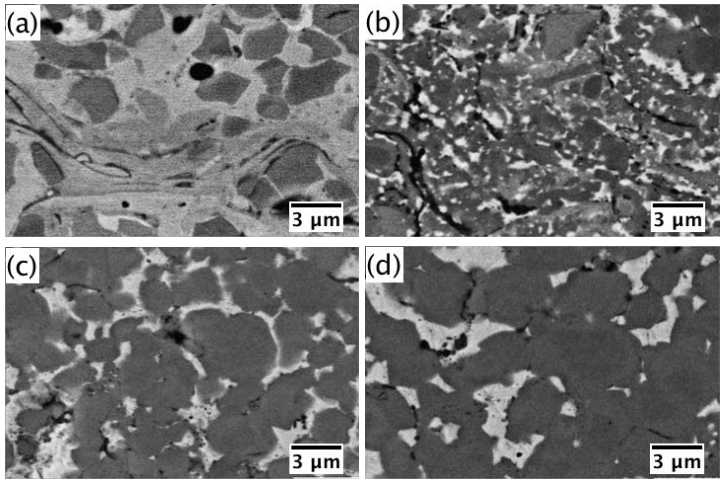

Figure 3.5: The microstructure of as-sprayed Cr_3C_2-NiCr coating (a) and the evolution of the microstructure after heat-treatment at 900 °C for 2 (b), 20 (c), and 60 days (d). Reproduced from ref. [28].

3.2.3 Thermally sprayed Cr_3C_2-WC-Ni

The development of the Cr_3C_2-WC-Ni feedstock composition stems more from individual empirical studies than from any systematic improvement and optimization of the composition. Thus, there is a lack of consistent studies about the interaction of these carbides. The historically relevant 70WC-24Cr_3C_2-6Ni composition is based on a patent by Koffskey et al. [18]. Occasionally, feedstock powders with essentially corresponding compositions are traded with the designations: WC–20'Cr_3C_2'–7Ni, WC–$(W,Cr)_2C$–Ni, or WC–NiCr [22]. The $(W,Cr)_2C$ designation is due to the formation of the Cr-rich W_2C carbide during feedstock powder consolidation at high sintering temperatures [21]. Hence, this composition is more than just a simple binary-carbide hardmetal. Figure 3.6 shows the microstructure of a 70WC-24Cr_3C_2-6Ni feedstock granule (a) and HVOF sprayed coating (b). The atomic mass-sensitive micrograph displays WC and Cr_3C_2 grains respectively with bright and dark gray-scale values.

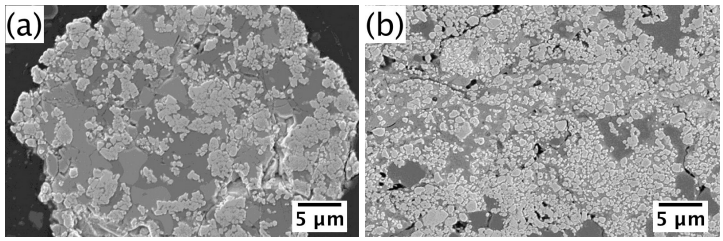

Figure 3.6: Electron microscopy micrographs of the cross-section of 70WC-24Cr_3C_2-6Ni feedstock granule (a) and HVOF sprayed coating (b). Reproduced from ref. [21].

The tribological performance of coatings sprayed from feedstock compositions corresponding to 70WC-24Cr_3C_2-6Ni have been studied previously [20–22, 104–106]. The composition has higher oxidation resistance at elevated temperatures than WC-CoCr

[104]. However, the room-temperature erosion [106], abrasion [105] and sliding wear [22] resistances are inferior to the WC-CoCr coatings. As intended by Koffskey [18], the composition's main industrial potential lies with high-temperature applications.
In recent years the focus has shifted towards compositions with higher Cr_3C_2 content in place of the relatively precious WC [24, 58, 107–109]. For example, the 45Cr_3C_2-37WC-NiCo composition (Oerlikon Metco 7500 series feedstock powder) contains a significantly higher Cr_3C_2/WC-ratio than Koffskey´s 70WC-24Cr_3C_2-6Ni composition. At room temperature, the HVOF and HVAF sprayed 45Cr_3C_2-37WC-NiCo coatings demonstrated higher resistance against sliding wear than 75Cr_3C_2-25NiCr [58]. However, the wear tracks of the 45Cr_3C_2-37WC-NiCo coatings tested at 700 °C displayed non-uniform tribolayer with oxidized WC grains, and therefore higher wear rate than the 75Cr_3C_2-25NiCr coating. Hence, there is a clear need to reduce the W alloying during further feedstock development. Zhou et al. [107] presented an experimental Cr_3C_2-WC-NiCoCrMo feedstock with a similar Cr_3C_2/WC-ratio. The resistance against sliding wear of the HVOF sprayed experimental Cr_3C_2-WC-NiCoCrMo coating exceeded the Cr_3C_2-NiCr reference both at room and high (450 °C - 650 °C) temperatures. Moreover, this experimental coating displayed a comparable high-temperature oxidation rate at 800 °C with Cr_3C_2-NiCr [108]. To conclude, although both the commercially available compositions, 73WC-20Cr_3C_2-7Ni and 45Cr_3C_2-37WC-NiCo have demonstrated inferior room temperature sliding wear resistances to WC-CoCr, they are however, still far superior to plain Cr_3C_2-NiCr. The vast majority of the wear testing has been performed with a sliding test apparatus against alumina counterparts. Therefore, more tribological testing is needed in order to develop a comprehensive understanding of the tribological potential of these coatings. Furthermore, the oxidation resistances of Cr_3C_2-rich coatings with various WC contents should be probed in the future.

4 Abrasive Wear

Wear is defined as damage to, or material loss from, a solid surface caused by relative motion between the surface and a counterbody. Abrasive wear, a subcategory of wear with vast economic importance, denotes damage induced by hard particles or high asperities sliding or rolling over the surface [1].

4.1 Classification of Abrasion

Abrasion can be roughly categorized into two-body or three-body abrasion according to the type of contact. Two-body abrasion occurs when a rigid abrasive counter-body slides over and scratches the wear surface [1]. An example of this process is the material loss achieved with abrasive sandpaper. In three-body abrasion, the freely moving particles are caught between two loaded surfaces, wherein the abrasive particles can roll freely [1]. This wear process occurs in e.g the jaw plates in a jaw crusher or when a mouldboard plough is drawn through sandy soil. Moreover, in other wear processes the formation of hard debris particles from the worn surface can also induce three-body abrasive wear. The material loss in three-body abrasion is markedly lower than in two-body abrasion [1]. This stems from the rolling motion of the abrasives between the loaded surfaces in the tribocontact [110].
Occasionally abrasion is sometimes further categorized into low-stress or high-stress abrasions [1]. In low-stress abrasion, the abrasive particles remain practically intact during the abrasion process. However, high-stress abrasion is characterized by fracturing of the abrasive particles under a heavy load. The most common physical interactions between abraded surfaces and sliding abrasive particles are presented in fig. 4.1 [110]. In microploughing, the surface is plastically deformed and the material only flows around the sliding particle, while no material is actually removed from the surface, see (a). When the surface is ploughed repeatedly the low cycle fatigue of the heavily-deformed surface layer causes material loss by microfatigue, see (b). If the attack angle of the abrasive particle is increased, the interaction between the abrasive particle and the surface transforms from microploughing to microcutting. In microcutting, chips of the material are removed by a mechanism that corresponds closely to machining, see (c). These above described physical interactions between the hard abrasive particle and the surface appear if the abraded material is relatively soft and ductile [111]. However, the abrasion process on a hard surface is significantly different; microcracking occurs when the abraded surface is brittle and thus incapable of absorbing the energy of the abrasion by plastic deformation, see (d). Ceramic materials, in particular, display microcracking under high contact pressures from the sliding particles [112].
Even though the above-described abrasion classifications are commonly used, there is some controversy about the usefulness of categorizing such complicated mechanical

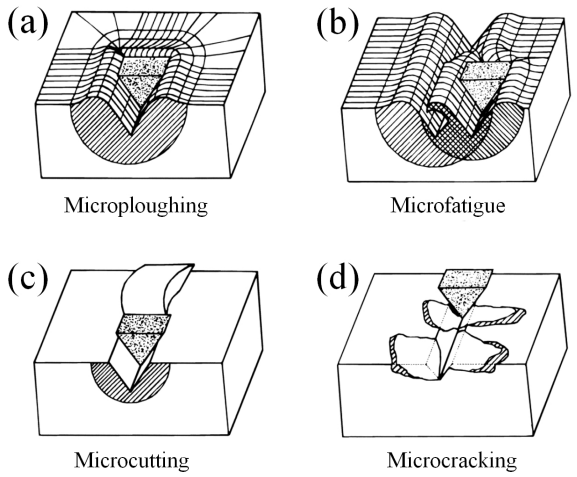

Figure 4.1: Schematic illustration of microploughing (a), microfatigue (b), microcutting (c), and microcracking (d) by Zum Gahr [110].

interactions into a few simplified categories [113]. In practice, various processes can occur simultaneously, which often makes the exact classification of an abrasive process challenging. Therefore, it is common practice to build specialized wear testing devices to probe abrasion in a particular industrial application.

4.2 Abrasion at High Temperatures

Much industrial processing equipment undergoes abrasive wear at elevated temperatures, e.g. sieves for screening of iron oxide sinter in the steel industry are exposed to high temperature abrasion [114]. The mechanisms that affect the abrasion processes at high-temperature are discussed below.

In metallic materials, thermally-induced dislocation migration at high temperatures reduces the hardness and work hardenability of the material. Moreover, abrasive particles, if they are subjected to intense heat, can also lose their strength [83]. This is significant because in abrasion it is mainly the hardness ratio between the surface and the abrasive particle that determines the wear rate [115]. Thus, any changes in this ratio due to an elevated temperature, for instance, alter the tribosystem [83]. Moreover, at elevated temperatures abrasive particles can penetrate and get stuck in the softened metal more readily. These mechanically-alloyed abrasive/metal layers can improve the wear resistance of the surface [83, 116, 117]. In fact, in some cases the wear resistance of metallic materials is actually improved at higher service temperatures.

Metal matrix composites (i.e. hardmetals, hardfacings, and cermets) offer the most intense wear protection against abrasion. The hard carbide phase, which usually makes up more than 40 wt.% of the composition, increases the hardness of the material and thus its resistance to the penetration of abrasive particles. Obviously, the penetration is prevented most efficiently if the carbide is relatively large compared to the width of the groove produced by the sliding abrasive [1]. At elevated temperatures, the softening of the metal matrix increases the width of the groove. Therefore, at high temperatures, coarse carbides are considered beneficial [83].

Various hardfacing compositions are used in high-temperature three-body abrasion conditions [42, 43, 118, 119]. Usually, these are composed of Fe, Ni or Co matrices with precipitated Cr_7C_3, or synthetic WC/W_2C carbides. Furthermore, hardfacings with more complex compositions are also used, e.g. the FeCrNbBWC alloy contains FeCr-carboborides together with NbC and WC hardphases [43]. In Fe-based alloys, the pronounced softening of the metallic phase occurs already at 500 – 650 °C [43, 118, 119], while the softening with Ni and Co alloys does not occur until considerably higher temperatures are reached. Given the softening of the metallic matrix, distinct breakage of carbides can occur due to insufficient mechanical support from the matrix [118]. Thus, the high-temperature abrasive wear resistance in Ni-based alloys is usually higher than in Fe-based alloys [119], and Co-based alloys display even more attractive abrasion resistance [43]. Also in high-temperature impact-abrasive conditions, the superiority of the Ni- and Co-based alloys over Fe-based alloys is significant [43, 118].

4.3 Abrasion of Thermally Sprayed Cr_3C_2-NiCr

Owing to their high volumetric content of hard carbides, hardmetals are renowned for their tremendous wear resistance. Both bulk [120] and HVOF sprayed [121] WC-Co hardmetals demonstrate high resistance against abrasion.
Several studies have been published in which the abrasion behaviors of various hardmetal coatings have been compared [23, 122 – 126]. The vast majority of these studies have been performed with an ASTM G65 abrasion testing rig, where the wear regime corresponds to low-stress three-body abrasion. HVOF sprayed Cr_3C_2-NiCr coatings have superior low-stress abrasion resistance to Ni-based self-fluxing alloys, hard-chrome coatings, and hardened steels; yet they are still far inferior to WC-Co hardmetals and to (Ti,Mo)(C,N)-NiCo cermets [122].
Kašparová et al. [23] studied the abrasion resistance of Cr_3C_2-NiCr in low-stress and high-stress conditions. Alumina particles were used as abrasives, and the load in both tribosystems was 22 N. The rotating counter-surface that was pressed against the sample was made out of steel (high-stress abrasion) or rubber (low-stress abrasion). In high-stress abrasion, the wear rates for Cr_3C_2-NiCr and WC-Co were 5.54 $\times 10^{-2} mm^3/m$ and 2.23 $\times 10^{-2} mm^3/m$, respectively. In low-stress abrasion (ASTM G65) the difference between these two compositions was even higher; wear rates were 8.72 $\times 10^{-3} mm^3/m$ and 1.80 $\times 10^{-3} mm^3/m$ for Cr_3C_2-NiCr and WC-Co, respectively.
The worn surface in Cr_3C_2-NiCr after low-stress abrasion displayed a smooth and polished appearance. Both the binder and the Cr_3C_2 phases were uniformly worn. In addition, the surface presented pull-outs and cracking of the carbides, the cracks were aligned perpendicularly to the abrasion rolling direction. However, no signs of selective binder removal were detected. After high-stress abrasion, the wear track of Cr_3C_2-NiCr displayed a plastically deformed rough surface with deep scratches. These rough wear tracks consisted of regions where large chunks of material had been removed during the abrasion process. Furthermore, debris from the abrasives was trapped in the cavities of the roughened surface. Thus, mechanical mixing appeared to occur in some degree during high-stress abrasion.
Perhaps surprisingly, even though the Cr_3C_2-NiCr composition is intended for high temperatures applications, there is a lack of research on the elevated temperature abrasion behavior and properties of this composition. The erosion resistance, however, has been studied at high temperatures [127 – 129]. At high temperatures (700 - 850 °C), the heat-induced microstructural changes in HVOF- and HVAF-deposited Cr_3C_2-NiCr coatings

contribute to erosion resistance [127, 129]. Wang et al. [127] proposed that with an as-sprayed coating at 300 °C, the erosion rate was lower than at room temperature due to the improved ductility of the coating. Also, Matthews [129] concluded that the enhanced ductility of NiCr binder has a marked influence on the erosion resistance at 800 °C. However, after a long dwell time at high temperature, the Ostwald ripened network of coarse carbides restricted the ductile response of a soft binder upon the impact of the particle; at 800 °C the as-sprayed HVOF coating displayed higher erosion resistance than heat-treated coatings (treated at 900 °C for 2 or 30 days) [129]. Therefore, the high-temperature erosion resistance of Cr_3C_2-NiCr coatings is governed by the rapid-heat-induced changes in the mechanical behavior of the binder phase and the slow coarsening of the carbide structure.

5 Materials and Methods

This chapter presents the materials studied in this work. It includes the descriptions of the powder compositions, the commercial designations of the powders, and the coating deposition processes. Moreover, the methodology describes in detail how these materials were characterized and subsequently probed.

5.1 Feedstock Powders and the Deposition of the Coatings

In this study, the coatings were deposited from both the commercially available and experimental feedstock powders by DJ-2700 hybrid HVOF, K2 HVOF, and M3 HVOF torches. The commercial designations, compositions, and size fractions of the feedstock powders are listed in table 5.1. The feedstock powders were manufactured by agglomerating and sintering. Moreover, powders C3 and C4 were subsequently post-treated with a plasma densification procedure. Powders C1 and C2 were chosen for this study, as they showed representative a&s powder morphologies and microstructures. These a&s powders differed by the size of carbides, C1 had coarser carbides than C2. Plasma densified C3 and C4 powders, however, showed distinctly different microstructures to a&s powders due the rapid melting and re-solidification of granules during densification treatment.
The experimental a&s powders, E20 and E10, were prepared at Fraunhofer IKTS (Dresden, Germany) by the following method. First, the starting constituents Cr_3C_2, WC and Ni, were milled in an aqueous suspension by an agitator ball mill until the required level of deagglomeration of the powders was reached. Then, the particles were granulated in a small-scale spray drier with a fountain nozzle setup. Finally, the granule consolidation was achieved by sintering at 1200 °C in an inert atmosphere. This process is described in more detail in Paper IV.
The deposition of the coatings was performed by KVT Kurlbaum AG (DJ), Fraunhofer IWS (K2) and Putzier Oberflächentechnik GmbH (M3). The spray parameters and deposition efficiencies are shown in table 5.2. The deposition efficiency (DE) values for various powders and processes provide useful information about the spray economics and have been published earlier in a more industrially-oriented journal [130], which is not considered as part of this work. In this work, the focus is solely on the properties of the coatings. Moreover, the M3 spraying parameters were not provided by the manufacturer. However, the properties of M3-sprayed coatings are considered to represent typical industrial quality HVAF coatings. The substrates were 10 × 10 cm sized austenitic DIN 1.4828 steel plates, which were grit blasted prior to the spraying process. In the following chapter, the coatings are identified by the deposition process and the feedstock powder, e.g. K2-C2.

Table 5.1: Powders and coatings studied in this work

Name	Commercial name	Composition (wt.%) WC	Cr_3C_2	binder	Size fraction (μm)	Spray torch
C1α	Durmat 251.007	-	75	25($Ni_{0.8}Cr_{0.2}$)	-45 +15	DJ,K2
C1β	Durmat 251.091	-	75	25($Ni_{0.8}Cr_{0.2}$)	-30 +5	M3
C2α	Experimental	-	75	25($Ni_{0.8}Cr_{0.2}$)	-45 +15	DJ,K2
C2β	Amperit 589.059	-	75	25($Ni_{0.8}Cr_{0.2}$)	-30 +10	M3
C3α	GTV 80.81.1	-	75	25($Ni_{0.8}Cr_{0.2}$)	-45 +15	DJ,K2
C3β	GTV 80.81.8-32	-	75	25($Ni_{0.8}Cr_{0.2}$)	-30 +5	M3
C4α	WOKA 7301	-	75	25($Ni_{0.8}Cr_{0.2}$)	-45 +15	DJ,K2
C4β	WOKA 7304	-	75	25($Ni_{0.8}Cr_{0.2}$)	-30 +10	M3
W1α	WOKA 7502	37	45	18(NiCoCr[1])	-45 +15	K2
E20	Experimental	10	70	20(Ni)	-45 +20	K2
E10	Experimental	10	80	10(Ni)	-45 +20	K2
		Laser post-treated coatings				
C4γ	WOKA 7303	-	75	25($Ni_{0.8}Cr_{0.2}$)	-45 +11	K2
W1γ	WOKA 7503	37	45	18(NiCoCr)	-45 +11	K2

[1] Ni: 62 wt.%, Co: 20 wt.%, Cr: 17 wt.%, and Fe: 1 wt.%

Table 5.2: Deposition parameters and deposition efficiencies [130]

	DJ Gas-fueled HVOF	K2 Liquid-fueled HVOF	M3 Gas-fueled HVAF
Torch	Metco DJ-2700 hybrid	GTV K2	Uniquecoat M3
Fuel	Ethene	Paraffin	Propane
Fuel flow	110 nlpm	24 l/h	-
Oxygen flow	250 nlpm	820 nlpm	-
Air flow	340 nlpm	-	-
Powder feed rate	40 g/min	110 g/min	130 g/min
Spray distance	230 mm	300 mm	-
Coating manufacturer	KVT Kurlbaum AG	Fraunhofer IWS	Putzier GmbH
Powder		Deposition efficiency (%)	
C1 (α)(β)	55(α)	36(α)	31(β)
C2 (α)(β)	55(α)	41(α)	49(β)
C3 (α)(β)	60(α)	42(α)	25(β)
C4 (α)(β)	55(α)	31(α)	51(β)
W1 (α)	60(α)	44(α)	
E20		48	
E10		48	

5.2 Post-Treatments

In order to simulate the heat-induced microstructural changes occurring over time at high service temperatures, the selected coatings were heat-treated at 800 or 900 °C for from 8 to 196 h. The heat-treatments were performed in an argon atmosphere to minimize the oxidation of the surface.

A laser post-treatment procedure was developed for this study. Unlike in the much-studied laser glazing process, wherein the high laser fluence melts the deposit, here the laser fluence was kept low to maintain the coating in a solid state throughout the post-treatment

process. This was done because during our previous studies with laser glazing, it was noticed that the partial melting of the coating leads to decomposition of the carbides, cracking of the coating, and in some cases even the detachment of the coating from the substrate.
During the laser post-treatment, the K2-C4γ and K2-W1γ coatings were irradiated with a high power direct-diode laser (Highlight 8000D, Coherent Inc.) at a wavelength of 975 nm in continuous wave mode. The rectangular laser beam size of 24×12 mm^2 was adjusted by an optical setup. The laser power of 3kW was kept constant, while the traverse velocity of the beam was varied in order to change the laser fluence. The laser post-treatment parameters are listed in table 5.3.

Table 5.3: Laser post-treatment parameters

Name	Velocity (mm/s)	Irradiance (W/mm^2)	Fluence (J/mm^2)
LT6	6	10.4	20.8
LT8	8	10.4	15.6
LT10	10	10.4	12.5
LT12	12	10.4	10.4

5.3 Material Characterization

The microstructures of the coatings were studied from the polished cross-sections with the Scanning Electron Microscope (SEM) (Zeiss Supra 40VP or NVision40, Zeiss, Germany) in both Back-Scattered Electron (BSE) and Secondary Electron (SE) modes. The SEM was equipped with a Focused Ion Beam (FIB) for sample preparation. Moreover, in selected samples the local chemical compositions in the cross-sections were investigated by Energy Dispersive X-ray spectroscopy (EDX) (Pegasus detector).
The phase compositions of the various feedstock powders and coatings were characterized by X-ray diffraction (XRD) with Cu-Kα-radiation in a Bragg-Brentano geometry (PANalytical Empyrean, Netherlands). The subsequent phase identification was done by PANalytical X'Pert High Score Plus software. To remove the oxide layer from the surface, the surfaces of the coatings were ground prior to XRD characterization.
The heat input during post-treatment may cause thermal shock, which can result in cracking of the coatings. Hence, in order to determine the crack patterns, dye penetration tests were performed on the post-treated surfaces (red dye on white developer).

5.3.1 Hardness Measurements

The microhardness values of the coatings were probed with a Vickers diamond indenter (FM-700, Future-Tech, Japan) at a load of 0.3 kg in carefully polished cross-sections. The results show the average values of 20 indents located between 50 – 200 μm below the surface of the coatings.
In order to characterize the mechanical properties of individual phases, nanoindentation tests were done on selected coatings by a TI900 Triboindenter (Hysitron, USA) with a Berkovich indentation tip. Here, both the isolated indents and the indentation grids of 650 indents per coating were placed in the cross-sections of the coatings. The isolated indents were done at a load of 10 mN. The indentation grids were performed at a load of 2 mN in a region about 20 μm below the coating surface. The obtained load-displacement

curves were processed to the hardness values by the method described in ref. [131]. The hardness of the grid indentation studied coatings is presented in the following as a frequency diagram. This grid indentation method has been previously described in refs. [132 – 134].

5.4 Wear Studies

The abrasion studies were done with a rotating steel wheel (Hardox 500) abrasion testing device with a constant flow of Ottawa sand (dry spherical silica particles), see fig. 5.1. This high-stress abrasion setup roughly resembles the ASTM B611 high-stress abrasion testing standard for bulk hardmetals. In addition, the abrasion resistances were studied while the coatings were heated to 400, 600, and 800 °C by induction heating. A typical high-temperature testing cycle consisted of a 1-min heating-up phase, 5-min wear-testing phase, and a 5-min cooling-down period. After the tests, the wear loss was determined by

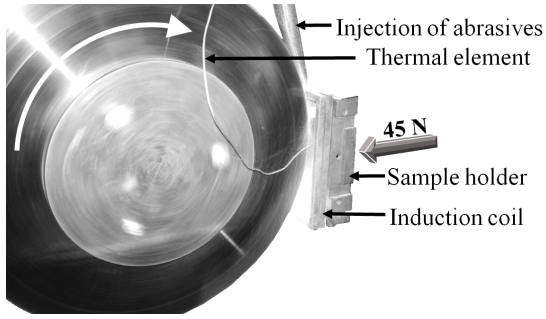

Figure 5.1: High-stress abrasion testing setup with induction heating element

weighing the samples. In order to compare the wear losses between different compositions, the volume losses were determined by using the nominal densities of the compositions. The wear test results present the average wear rate (mm^3/m) values of three individual tests. The testing parameters are listed in table 5.4

Table 5.4: High-stress abrasion testing parameters

Abrasion regime	High-stress
Counterbody	Hardox 500
Wheel diameter	220
Wheel width (mm)	13
Load (N)	45
Sliding distance (m)	300
Sliding speed (m/s)	1
Temperature (°C)	22, 400, 600, 800
Abrasive	Ottawa silica sand
Particle size	200 – 300 μm
Abrasive flow (g/min)	150

6 Results and Discussion

The main results from publications I-V are divided into four sections in this chapter. The first section (6.1) presents the microstructures and wear properties of the commercially available 75Cr_3C_2-25NiCr coatings. The wear resistances of as-sprayed and heat-treated coatings were studied at room temperature and at 800 °C. The second section (6.2) introduces the novel laser treatment procedure, which improves the room temperature wear resistance of Cr_3C_2-NiCr due to particle hardening through Cr_3C_2 precipitates. The third section (6.3) deals with WC-alloyed Cr_3C_2-based coatings and compares the experimental 70Cr_3C_2-10WC-20Ni and 80Cr_3C_2-10WC-10Ni coatings with the commercially available 37Cr_3C_2-45WC-NiCo and 75Cr_3C_2-25NiCr coatings. In the fourth section (6.4), the already introduced laser post-treatment was used to tailor the microstructure of the as-sprayed 45Cr_3C_2-37WC-NiCo coating by precipitating Cr-rich $(W_{1-x}Cr_x)_2C$ carbides from a Cr, W, and C supersaturated binder.

6.1 Characteristics of the Cr_3C_2-NiCr Coatings

The microstructures and wear properties of the state-of-the-art 75Cr_3C_2-25NiCr coatings are presented here. The properties of these commercial coatings are regarded as an industry benchmark for the further development of Cr_3C_2-based hardmetal coating. An overview is given here of the influence the feedstock powder and spray process has on both the microstructures and the high-stress abrasion resistances of the coatings. Because 75Cr_3C_2-25NiCr coatings are the major hardmetal composition for high temperatures, the effects of elevated service temperatures in the microstructures were simulated by various heat-treatments. Furthermore, the abrasion tests were performed at 800 °C. The results presented in this chapter are based on publications I and II.

6.1.1 Structures of the feedstock powders

The microstructures of the commercially available Cr_3C_2-NiCr feedstock powders are presented in fig. 6.1. The atomic mass sensitive BSE-micrographs of the powder granule cross-sections display the Cr_3C_2 carbides as dark gray-scale values and the NiCr binder as bright gray-scale values. Powders C1 (a)-(b) and C2 (c)-(d) have been manufactured by the a&s process. Both powders consist of a chromium carbide skeleton, which is only partially embedded into the metallic NiCr binder and thus the powder granules show high intragranular porosity. Furthermore, cracks are visible in the Cr_3C_2 grains. The main difference between the C1 and C2 feedstock granules is the size of the Cr_3C_2 grains; the carbides in the C2 granules are smaller than in the C1 granules. The corresponding microstructures are typical for a&s feedstock powders, and similar granule structures have been reported previously in refs. [11, 57, 59, 100].

The distinct feature in the plasma-densified powder C3 (e) is the presence of both hollow and dense granules. These granules are heterogeneous in morphology and extent of densification between the particles. Moreover, the cross-section of the C3 granule presents oxides, seen as dark entities in (f). The plasma-densified powder C4 (g)-(h) shows spherical and dense granules with wide carbide size-distribution. The vast variation in the carbide size in both plasma-treated powders is due to dissolution, and possibly even to the peritectic decomposition of Cr_3C_2 during the heating-up phase in the plasma treatment, which is followed by carbide precipitation as the granules cool down. Furthermore, various precipitated fine carbides display brighter gray-scale values than the coarse primary carbides, indicating variations in the stoichiometry. Matikainen et al. [57] found the presence of Cr_3C_2, Cr_7C_3, and metastable Cr_3C_{2-x} (wherein, $0 \leq x \leq 0.5$) from corresponding plasma-densified powders. These findings illustrate the rapid cooling of the granules after plasma treatment.

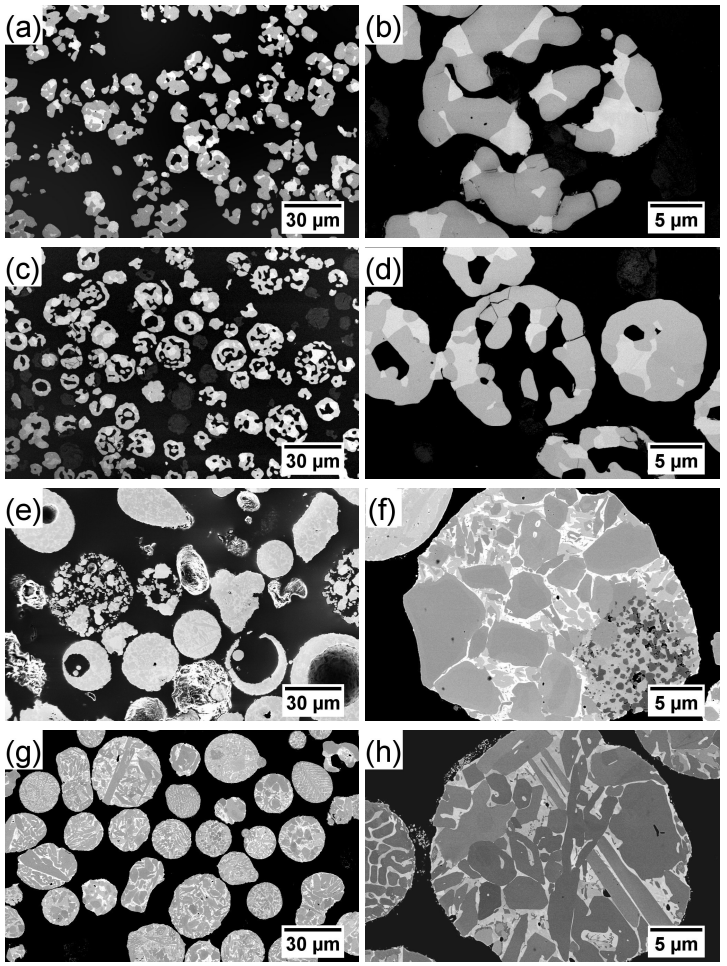

Figure 6.1: Cross-sections of the C1β (a,b), C2β (c,d), C3α (e,f), and C4α (g,h) feedstock powders [Publication I].

6.1.2 Structures and properties of the coatings

The microstructures of the as-sprayed DJ-C1 (a), M3-C1 (b), DJ-C4 (c), and M3-C4 (d) coatings are displayed in fig. 6.2. These micrographs show the impact that the feedstock powders and the spray-process selection have on the as-sprayed microstructure. The micrographs reveal that the microstructures of the corresponding feedstock granules are still clearly distinct from each other in the as-sprayed microstructures. The a&s feedstock sprayed coatings, DJ-C1 and M3-C1, display uniform carbide size distribution and high binder content. The high binder content indicates the loss of some of the carbide phase during deposition of the coating. This is often connected to the dissolution of carbides and selective carbide rebounding [45, 69]. Recently, Matikainen et al. [57] reported higher carbon losses in HVAF sprayed coatings than in HVOF sprayed coatings when a&s powder was used. Especially the use of feedstock granules with non-homogeneous carbide distribution and coarse carbide size were considered to result in pronounced selective carbide rebounding. Moreover, also signs of selective particle deposition, wherein granules with low metallic content rebound, were characterized in HVAF deposited coatings [57]. Here, the carbon content losses in the DJ-C1 and M3-C1 coatings are 1.5 and 2.5 mass fraction-%, respectively [Publication I]. Thus, these results also indicate that HVAF spraying of a&s feedstock induces more intense selective carbide rebounding than HVOF spraying, due to the higher kinetic energy of the particles.
The plasma-densified powder sprayed coatings DJ-C4 and M3-C4 show wide carbide size-distribution and high carbide content. Thus, the selective carbide rebounding is clearly hindered in the densified granules, wherein the carbides are well embedded in the binder. The spraying-induced carbon losses for DJ-C4 and M3-C4 are only 0.3 and 0.2 mass fraction-%, respectively [Publication I]. Hence, they are almost an order of magnitude smaller than in a&s feedstock sprayed coatings. Matikainen et al. [57] reported similar behavior in coatings sprayed from plasma-treated feedstock powders.
A distinctive feature in the thermally sprayed hardmetal coatings is the decomposition and dissolution of the carbides [70]. In the BSE-micrographs, this is reflected in variations of the gray-scale values in the binder phase. The high content of residual carbide-forming elements, namely Cr and C, converts the binder phase to a darker gray-scale. Typically these Cr- and C-rich regions appear in the microstructure as wavy patterns, because these regions represent the splat boundaries. The HVOF sprayed coatings DJ-C1 and DJ-C4 display markedly more noticeable dark wavy patterns than the HVAF sprayed M3-C1 and M3-C4. It was assumed that image analysis from BSE-micrographs of as-sprayed and heat-treated coatings was sufficient to determine the extend of carbide dissolution and reprecipitation, in order to interpret the variations in abrasive wear response.
Spraying the feedstock with an HVOF torch dissolves the carbides and thus changes the microstructure of the feedstock powders more than the colder HVAF torch does. This tendency has been reported before in refs. [57, 60, 61]. Another noticeable difference between the HVOF and HVAF coatings is the latter's higher density. The porosities of the DJ-C1 and DJ-C4 coatings are both roughly 1 vol.% [Publication I]. In the HVAF sprayed M3-C1 and M3-C4 coatings, however, the porosities are below 0.5 vol.% [Publication I]. This is attributed to the high kinetic energy of the impacting particles during HVAF spraying, which induces a peening effect and thus densifies the underlying coating.
The heat-treated DJ-C1 coatings are shown in fig. 6.3. The microstructure of the coating heat-treated at 400 °C for 5 min (a) displays essentially as-sprayed features, wherein the residual carbide-forming elements are uniformly distributed in the binder. The onset of chromium carbide precipitation is visible in the coating soaked at 600 °C for 5 mins (b). The further growth and coalescence of carbides are present in the coating soaked at

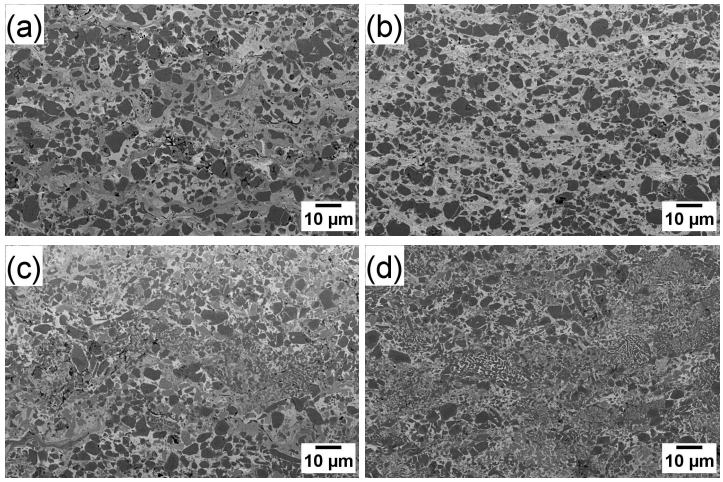

Figure 6.2: BSE-micrographs of the as-sprayed DJ-C1 (a) M3-C1 (b) DJ-C4 (c), and M3-C4 (d) coatings [Publication I].

800 °C for 8 h (c). After a long soak (196h) at 900 °C, the microstructure of the coatings shows coarse carbides, as reported previously by Matthews et al. [28]. As C and Cr from the binder are consumed by the growing carbides, the binder phase is represented with a bright gray-scale value. Hence, the heat-treatment drives the microstructure towards Cr_3C_2-Ni(Cr) equilibrium [98].

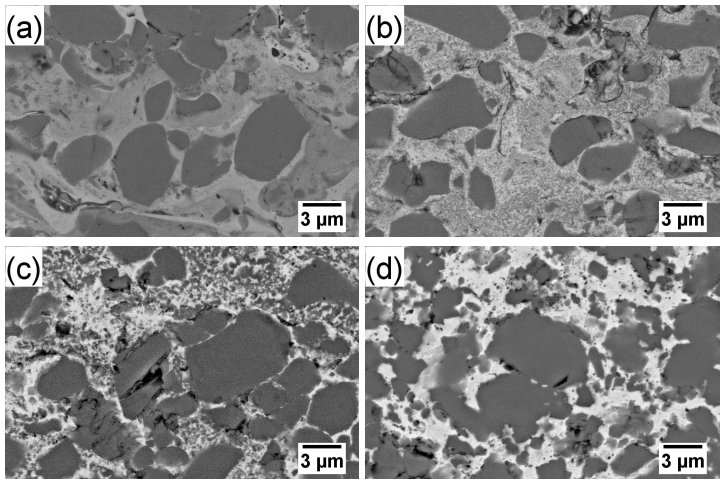

Figure 6.3: Micrographs of DJ-C1a coating after heat-treatment of 5 min at 400 °C (a), 5 min at 600 °C (b), 8 h at 800 °C (c), and 196 h at 800 °C (d) [Publications I and II].

The microhardnesses of the as-sprayed and heat-treated (8 h/ 800 °C) DJ-C1, K2-C1, and M3-C1 coatings are shown in Fig. 6.4 [Publication I]. The microhardness of thermally sprayed coatings is usually attributed to the composition, porosity, and the residual stresses in the coating [135]. Here the slightly increasing microhardness values, in the order DJ-K2-M3, are considered to have stemmed from the compressive residual stresses

induced by the particle peening. Presumably, the M3 torch yields coatings with the highest compressive stresses, as the velocities of the impacting particles are lowest in the gas-fueled HVOF torch (DJ) and highest in the HVAF torch [57, 136]. After the heat-treatment, the residual stresses are relaxed in the coatings and the microhardness values go down. Interestingly, the deposition process itself does not play a major role in the microhardness after the heat-treatment. In fact, M3-C1 has a slightly lower hardness value than the K2-C1 coating after heat-treatment, which is attributable to the low carbide content.

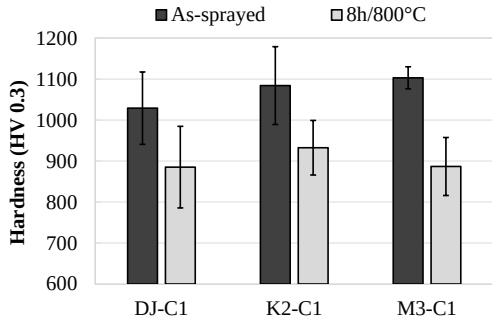

Figure 6.4: Hardness of as-sprayed and heat-treated (8h/800 °C) coatings [Publication I].

The reason for the reduction in the microhardness induced by the heat-treatment was further probed with isolated nanoindentations. Fig. 6.5 presents the results of indentations made on the binder and the carbide grains of as-sprayed and heat-treated coatings [Publication II]. The heat-treatment does not alter the hardness of the carbide phase; carbides in as-sprayed and heat-treated coatings show similar nanohardness values of 30 GPa. However, the as-sprayed binder has considerably higher hardness values and lower ductility values than the heat-treated binder. Murthy et al. [137] found corresponding behavior for fairly similar coatings and validated the heat-induced binder hardness drop to grain growth of nano-sized Ni-grains and reduction of solid solution strengthening. The residual carbide-forming elements, C and Cr, act as solid solution strengtheners in the Ni-lattice of the as-sprayed coating. When these elements precipitate to carbides, the degree of solid solution strengthening is reduced. Fig. 6.5 (b) and (c) show the indents in an as-sprayed and a heat-treated binder, respectively. The precipitated carbides with diameters of 200-500 nm in the heat-treated binder are too coarse to strengthen the Ni-lattice through particle hardening. Therefore, the nanohardness of the binder, and consequently the microhardness of the coating, are reduced during heat-treatment. However, by using the optimal heat-treatment procedure the Ni-lattice can be strengthened with small coherent carbides [137].

6.1.3 Wear resistance of the coatings

The results of the high-stress abrasion tests performed at room temperature are presented in Fig. 6.6 (a) [Publication I]. The influence of the spray process on the wear resistance is clear; there is a distinct trend in improved wear resistance from DJ through K2 to M3 for all the coatings. This trend is attributed to the ductility of the binder phase. As shown in fig. 6.5 (a), the carbide dissolution promoted by the spraying results in

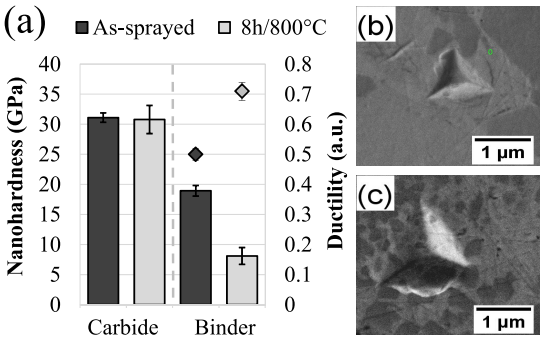

Figure 6.5: Nanohardness values (presented by bars) of the carbide and binder phases of as-sprayed and heat-treated (8h/800 °C) coatings and the ductility of the binder (presented by the diamond-shaped markers) (a). BSE-micrographs from the indents in as-sprayed (b) and heat-treated (c) binder [Publication II].

embrittlement of the binder. Moreover, the coatings deposited by the ethene-fueled DJ torch exhibited the highest dissolution of the carbides. In contrast, the M3 torch sprayed coatings were characterized by the highest carbide loss and also by hindered carbide dissolution. Therefore, these results indicate strongly that the high-stress abrasion resistances of the as-sprayed Cr_3C_2-NiCr coatings are governed by the binder properties. The C4 feedstock sprayed coating show the lowest wear rates at room temperature. This is attributed to low porosity and high carbide content in the coating. Moreover, due to dense feedstock particles, it is possible that the degree of in-flight carbide dissolution is lower in plasma-densified than in a&s powders. In C4 feedstock sprayed coatings this would yield binder with low Cr and C contents and thus result in ductile mechanical response when loaded with abrasive particles.

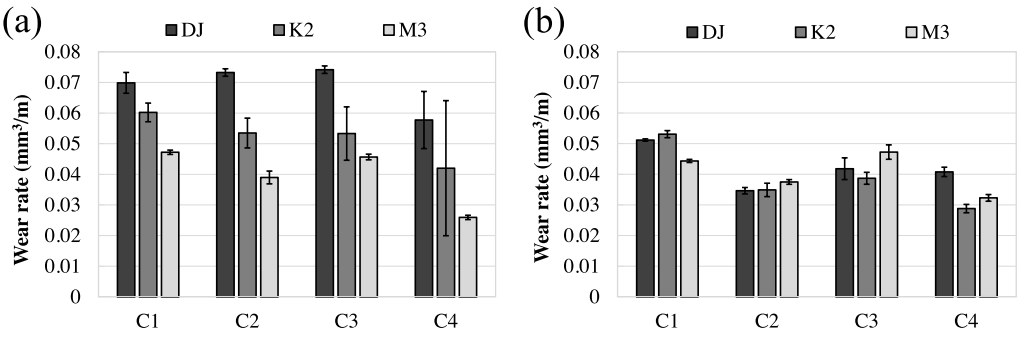

Figure 6.6: High-stress abrasion wear rates of as-sprayed (a) and heat-treated (8h/800 °C) (b) coatings tested at room temperature [Publication I].

Further proof for this reasoning is shown in fig. 6.7 [Publication II], wherein the as-sprayed DJ-C1 wear tracks are presented from the top, in (a) and (b), and from the cross-section (FIB cut sections), in (c) and (d). The wear track in (a) shows heavy plastic deformation, a partially fractured surface, and sparsely scattered scratches. It is unclear whether these scratches stem from the ploughing or from the microcutting of the sliding abrasive particles [138]. Moreover, a crack propagating through the brittle binder can be seen in

(b). Cracks were also found in the sub-surface zone, as presented in (c) and (d). These sub-surface cracks propagated through the pristine as-sprayed binder, which was not plastically deformed during abrasion. Therefore, the material loss from the high-stress abrasion was attributed to the plastic flow of the material and the brittle fracture of the supersaturated binder. In addition, the propagation of the subsurface cracks is considered to increase material loss through the chipping away of large chunks.

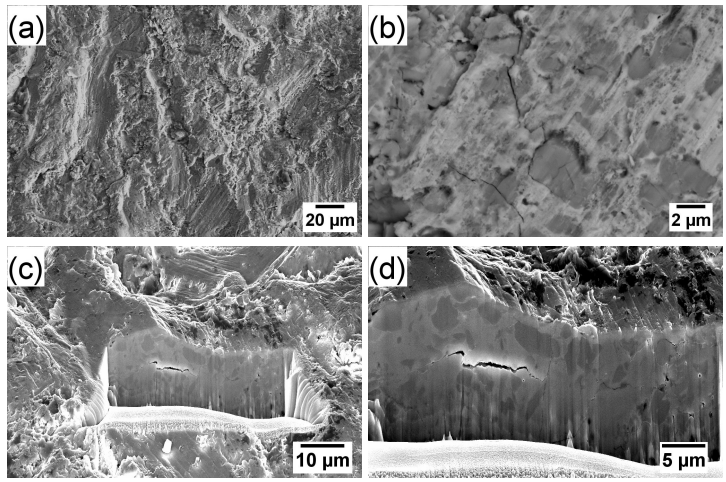

Figure 6.7: SE (a), BSE (b), and FIB-cut SE (c,d) micrographs of the wear tracks of as-sprayed coatings [Publication II].

The impact of the heat-treatment on abrasive wear resistance is demonstrated in fig. 6.6 (b) [Publication I]. All of the studied coatings display lower wear rates in the heat-treated state than in the as-sprayed state. The improvement in ductility induced by carbide precipitation (shown in fig. 6.5) is considered to be the main reason for the increased high-stress abrasion resistance. This is further illustrated by the fact that the gain in wear resistance from heat-treatment was highest in the DJ coatings (50 to 100%) and lowest in the M3 coatings (-20 to 10%). Because the spray-induced brittleness in the binder does not dominate the wear process after the heat-treatment, these results provide an overview on the dependence of abrasion resistance on the carbide phase. For example, here the C4 coatings show distinctly lower wear rates than the C1 coatings, that can be attributed to higher carbide content in C4 (75 vol.%) than in C1 (65 vol.%) [Publication I]. The wear tracks of the heat-treated coatings are presented in fig. 6.8. Compared to the brittle as-spray coatings, the wear tracks in the heat-treated coatings have a pronounced ductile character. The scratches on the surface show a higher degree of wedge formation, indicating an abrasion mode dominated by ploughing [138]. In addition, the cracks are mainly visible in the carbides and do not propagate through the binder phase.
The high-stress abrasion wear rates at 800 °C are presented in fig. 6.9. These results compare the K2 sprayed coatings after various heat-treatments. As expected, at elevated temperatures the material loss was increased; at 800 °C the wear rates are 50-100% higher than at room temperature. This is validated by the thermal softening of the binder and carbides [83], and thus an increased abrasion rate according to Rabinowicz's wear equation [139]. The long (100h/ 800 °C) heat-treatment yielded equalization of the microstructure, and the choice of feedstock powder resulted in only negligible differences

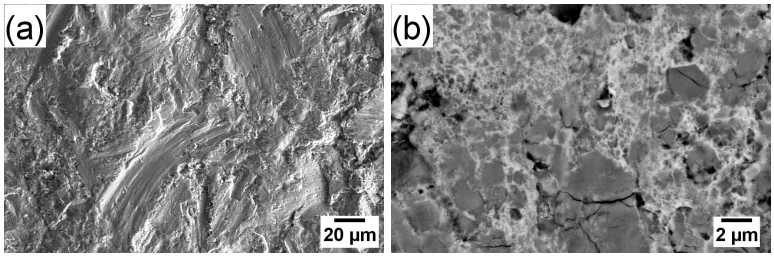

Figure 6.8: SE (a) and BSE (b) micrographs of the wear tracks of heat-treated (8h/800 °C) coating [Publication II].

in abrasion resistance. These wear tracks had a similar ductile appearance as the wear tracks of the heat-treated coatings tested at room temperature [Publication I].

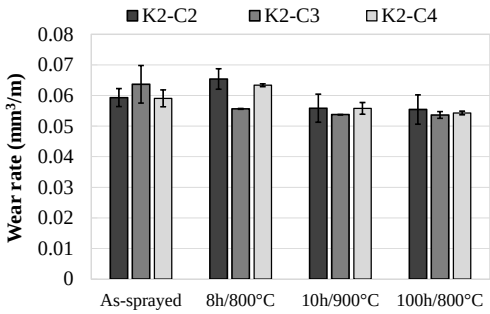

Figure 6.9: High-stress abrasion wear rates at 800 °C of K2-C2, K2-C3, and K2-C4 coatings after various heat-treatments [Publication I].

6.1.4 Conclusions

Four commercially available feedstock powders were deposited by gas- and liquid-fueled HVOF and HVAF torches. The microstructures of the as-sprayed coatings displayed features that stemmed from the feedstock powder consolidation method and the deposition process for the coating. These features mainly included the carbide size-distribution and the carbide dissolution during spraying. The heat-treatment changed the microstructure by precipitating the residual carbide-forming elements as chromium carbides. Even though the as-sprayed coatings displayed significant differences in abrasion resistance at room temperature, after heat-treatment the equalization of the microstructure evened out the differences. In the abrasion tests performed at elevated temperatures (800 °C) there were only minimal differences between the wear resistances of the different coatings. Thus the heat-treatment leads to a recovery of the phase composition through precipitation of dissolved carbide grains. The growth of the carbides with extended heat-treatment led to the formation of similar coating microstructures across the range of feedstock manufacturing routes and deposition techniques.

6.2 Characteristics of the Laser Post-Treated Cr_3C_2-NiCr Coatings

The previous section studied the influence of long-term heat-treatment on the high-stress abrasion resistance of Cr_3C_2-NiCr coatings, and showed that the heat-treatment improved the coating's high-stress abrasion resistance. However, the chromium carbides, which precipitated in the binder during the heat-treatment had diameters of well over 100 nm. Therefore, these precipitates were regarded as being too coarse to provide particle hardening in the Ni-lattice. Laser post-treatment had been utilized previously in other studies to melt the hardmetal coating [32–41]. The main aim of this remelting process was to reduce the as-sprayed coating's porosity and increase its corrosion protection capacity. This section describes how a different laser post-treatment procedure was used to precipitate nano-sized carbides in the binder of HVOF sprayed $75Cr_3C_2$-25NiCr coatings. Unlike in previous studies, with our laser post-treatment the coating remains in a solid state throughout the entire post-treatment process.

6.2.1 Structures and properties of the coating

The subsurface zones of the laser post-treated coatings are presented in fig. 6.10. The thermal treatment by laser irradiation has the greatest influence in the region close to the irradiated surface. The as-sprayed K2-C4 coatings have a similar gray, Cr- and C-rich binder as presented in the previous section. However, the coating post-treated with the 10.4 J/mm^2 laser fluence (b) has small precipitated carbides in the binder. The precipitates are clearly augmented after the coating was treated with 15.6 J/mm^2 (c). Furthermore, the coating treated with the highest fluence, 20.8 J/mm^2, (d) exhibits a similar Ostwald-ripened carbide structure and a bright, essentially C-free, binder as was exhibited by the coating which had been heat-treated in a furnace for 196h at 900 °C, see fig. 6.3.

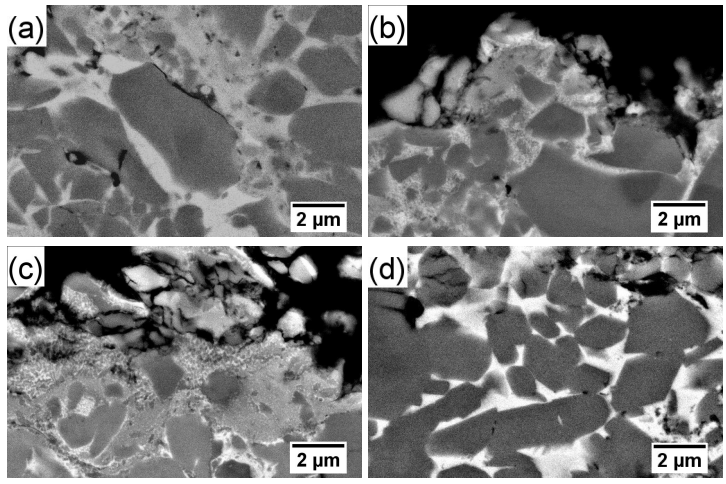

Figure 6.10: BSE-micrographs of the as-sprayed coating (a) and after laser post-treatment with fluences of 10.4 J/mm^2 (b), 15.6 J/mm^2, (c) and 20.8 J/mm^2 (d). The micrographs were taken 20μm below the surface [Publication III].

Because the BSE-images are not of a sufficiently high resolution to probe the size of the fine precipitated carbides, In-Lens micrographs of the as-sprayed and laser post-treated

binder are provided in fig. 6.11. The as-sprayed binder in (a) shows the Cr- and C-rich binder region without any precipitated carbides. However, fine nanosized precipitates are visible in the binder treated with the 10.4 J/mm^2 laser fluence. The precipitate size is in the range of 10-100 nm. Murthy et al. [137] speculated that this was close to the optimal particle size needed in order to restrict the migration of the dislocations and thus strengthen the Ni-lattice. If the precipitated carbides were to grow any further it would enable dislocation migration through the Orowan-process, wherein incoherent carbides are circumvented [140].

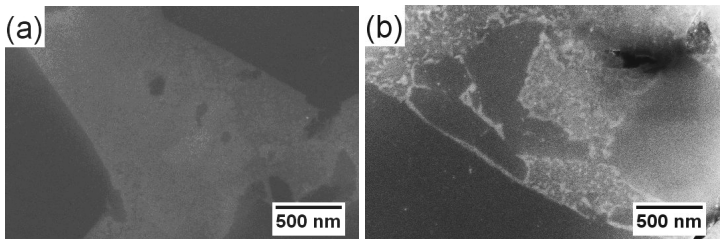

Figure 6.11: In-Lens SE-micrographs from the cross-section of as-sprayed (a) and 10.4 J/mm^2 laser fluence post-treated coating. The micrograph (b) was taken 50μm below the surface.

6.2.2 Wear resistance of the coatings

The high-stress abrasion resistance of the laser-tailored microstructures is shown in fig. 6.12. The WC-CoCr coating (dashed line) is regarded as the industry benchmark for the best abrasion resistance. The wear rate of the as-sprayed Cr_3C_2-NiCr coating is over 500% higher than that of the WC-CoCr reference coating. This vast difference in wear rate validates the fact that WC-CoCr serves for the vast majority of purely abrasion-protection applications. Kašparová et al. [23] presented roughly comparable differences in the wear rates of high-stress abrasion tested HVOF sprayed Cr_3C_2-NiCr and WC-CoCr coatings. The improved wear resistances of the laser-tailored microstructures can be seen by

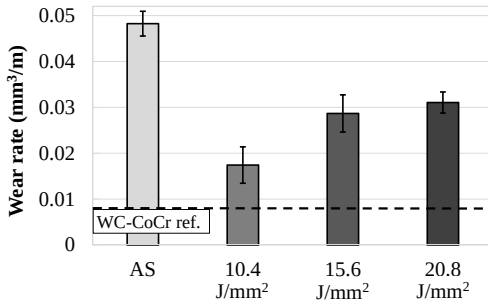

Figure 6.12: High-stress abrasion wear rates at room temperature for as-sprayed (AS) and laser treated (10.4 J/mm^2-20.8 J/mm^2) coatings [Publication III].

comparing their wear rates against the as-sprayed coating. The reduction in wear rate is most noticeable in the 10.4 J/mm^2 treated coating, whose wear rate was over 60% lower than the as-sprayed coating. This significant improvement in wear resistance is attributed

to the optimal particle hardening of the binder phase, as was shown above in fig. 6.11(b). Any further increase in the laser fluence yields coarser precipitates. Thus, the 30-40% lower wear rate in the 15.6 J/mm^2 and 20.8 J/mm^2 treated coatings is merely due to the improved ductility of the binder.

6.2.3 Laser-induced cracking of the coating

In order to study the cracking induced by the post-treatment, the surfaces were inspected using the dye penetrant method. This gives a rough estimate of the corrosion protection potential of the laser-treated coatings. The penetration inspection exposed cracks on the surface treated with the low 10.4 J/mm^2 fluence. However, the coatings treated with the higher fluences present pristine crack-free surfaces [1]. The exposed cracks are in parallel with the direction of the laser's movement. As the fluence was controlled by the laser's traverse velocity, this meant that while the laser irradiance was kept at a constant level (10.4 W/mm^2), the traverse velocity was highest (12 mm/s) during the 10.4 J/mm^2 fluence treatment and lowest (6 mm/s) during the 20.8 J/mm^2 fluence treatment. Therefore, the cracks are thought to propagate because of the high thermal stress levels, which were induced by the steep temperature gradient during relatively fast treatment by the laser beam.

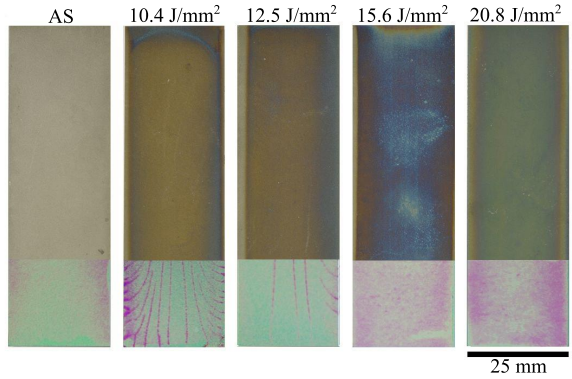

Figure 6.13: The inspection of the as-sprayed and laser-treated surfaces. Overlaid photographs of the dye penetration-treated surface (bottom) reveals cracking of the coating due to laser treatment [Publication III].

6.2.4 Conclusion

The microstructures and high-stress abrasion resistances of the laser post-treated coatings were studied. The increased wear resistance was especially pronounced with the coating treated at the fluence of 10.4 J/mm^2. This was due to the small nano-sized precipitates that resulted in particle hardening in the binder phase. However, the fastest laser traverse velocity led to cracking of the deposit, which indicates that these coatings have less potential to be used in corrosion protection applications. With the lower laser traverse

[1] The residuals of the red dye on the surface of the 15.6 J/mm^2 and 20.8 J/mm^2 fluence treated coatings were due to the rough as-sprayed surface topography

velocities, the number of cracks was reduced, but the reduced velocity resulted in coarser precipitates and thus higher wear rates.

6.3 Characteristics of the Cr_3C_2-WC-Ni Coatings

Section 6.1 demonstrated that 75Cr_3C_2-25NiCr systems approach thermodynamical equilibrium during heat-treatment [Publication I and II]. After prolonged service at high temperatures, the carbide dissolution induced by the initial structure of the feedstock powder and the spraying plays only a minor role in the microstructure of the coating. Therefore, neither the powder consolidation technique (sintering or plasma densification) nor the spray process (gas-fueled HVOF, liquid-fueled HVOF, and gas-fueled HVAF) have a significant influence on the abrasion resistance of the coating after heat-treatment or prolonged service at high temperatures.
The next aim of this work was to improve the technical performance of the coating by WC alloying. The currently available commercial binary carbide coatings have close to an equal Cr_3C_2/WC-ratios. In these tests, the coating K2-W1 is taken to represent such commercially-available 45Cr_3C_2-37WC-NiCoCr and is used as a reference. In this section, two experimental compositions with reduced WC additions are studied: 70Cr_3C_2-10WC-20Ni (E20) and 80Cr_3C_2-10WC-10Ni (E10). Both of these contain only 10 wt.% of WC, which is considerably lower WC content than in any of the commercially available Cr_3C_2-WC spray feedstock compositions produced so far. In addition, in order to probe the role that the carbide content has in high-temperature abrasion resistance, the binder content was set to 20 wt.% and 10 wt.% in E20 and E10, respectively.

6.3.1 Feedstock powders

The granule morphologies (SE-image) and cross-sections (BSE-image) of the W1α, E20, and E10 powders are presented in fig. 6.14. In the BSE-images, the WC grains appear as bright entities. The commercial W1α has dense granules in which both the carbides, WC and Cr_3C_2, are well embedded into the binder phase. The WC grains are relatively coarse and exhibit a wide grain size distribution. Similar granule structures have been presented previously in refs. [58, 109]. In the experimental E20 and E10 powders, the high intragranular porosity in the granules is visible, while the Cr_3C_2 skeleton surrounds the binder, see (d) and (f). Moreover, the sub-micron sized WC grains are uniformly distributed throughout the granules.
Fig. 6.15 presents the elemental mapping of an E20 granule. The distribution of Cr and W is presented in (b) and (c), respectively. The elemental mapping reveals that during the sintering step of the agglomerated powder, W is diffused into the binder and the rim-section of the Cr_3C_2 grains. The presence of W in Cr_3C_2 is also confirmed by XRD patterns in Fig. 6.17.

6.3.2 Structure and properties of the coatings

The microstructures of the as-sprayed and heat-treated (8h/800 °C) Cr_3C_2-WC-Ni coatings, deposited by the K2 torch, are presented in fig. 6.16. The as-sprayed microstructures display similar features to the corresponding feedstock powders. The K2-W1 coating has a high 20 vol.% WC content [Publication IV], which closely corresponds to the nominal composition of the W1a powder. Hence, the coarse WC grains in K2-W1 exhibited no significant selective carbide rebounding during spraying of the coating. In addition, the

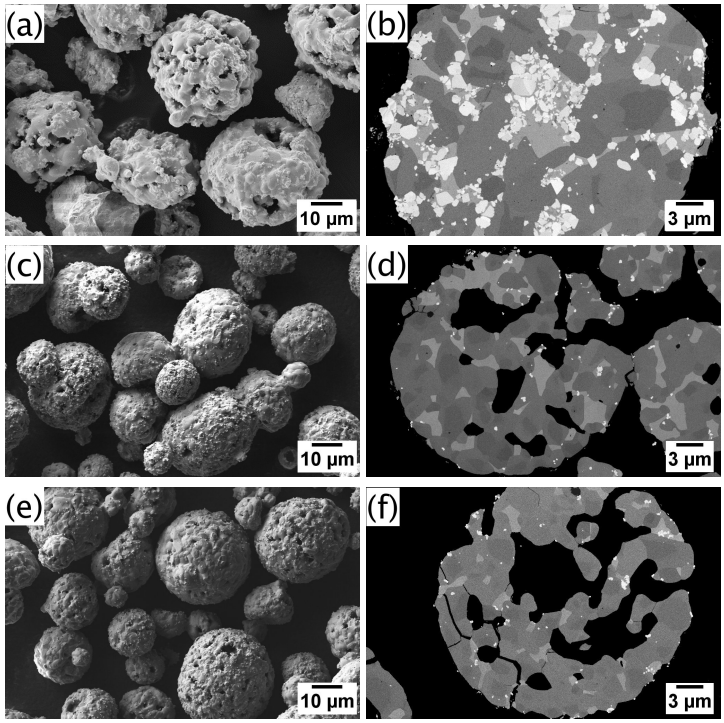

Figure 6.14: Morphologies (left column) and cross-sections (right column) of the W1α (a,b), E20 (c,d), and E10 (e,f) feedstock powders [Publication IV].

porosity level in the K2-W1 coating was relatively low; only 0.4 vol.% [Publication IV]. This high density is attributed to high inertia and the intense peening effect of the heavy WC-containing granules during the deposition process. Similarly dense microstructures have been presented previously in refs. [58, 107, 109].

In both the E20 and E10 coatings, the sub-micron sized WC grains are uniformly distributed throughout the binder phase. The WC content in these experimental coatings is only 2 vol.%. Therefore, the low volumetric content of plain WC grains is not expected to significantly increase the hardness or abrasion resistance of the coating by introducing a second, hard and wear-resistant carbide. Moreover, the aforementioned core-rim structured carbides, shown in the feedstock powder cross-sections, are clearly visible in the as-sprayed coatings. The impact of the binder content on the structure of the experimental coating is distinct; E10 (10 wt.% of binder) shows microcracks and poorly embedded carbides, while E20 (20 wt.% of binder) displays the same kind of dense structure as the commercially available $75Cr_3C_2$-25NiCr coatings shown previously in fig. 6.2. The porosities for the E20 and E10 coatings are 1.2 and 1.8%, respectively [Publication IV]. Thus, the low binder content in the E10 powder led to suppressed plastic deformation during the impact of the splat, which is reflected as low density in the coating. Similar conclusions about the detrimental effects of a high carbide content during spraying have been presented earlier by Chivavibul et al. [141].

The heat-treated coatings in figs. 6.16 (b), (d), and (f) display similar carbide precipitates in the binder phase as did the $75Cr_3C_2$-25NiCr coatings in fig. 6.3(c). The dark gray-scale values in these precipitates correspond to the gray-scale values of chromium carbides. This indicates that the nearly all of the residual W remained in the binder during the

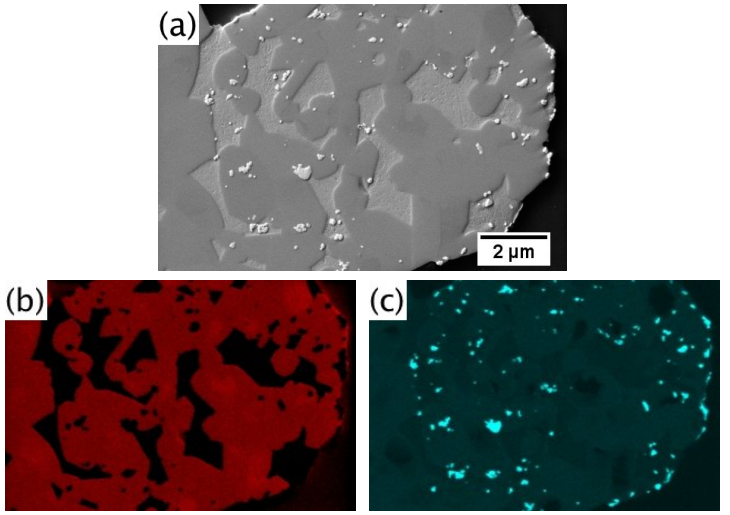

Figure 6.15: SE-micrograph (a) and elemental mapping of Cr (b) and W (c) from a granule of E20 powder [Publication IV].

heat-treatment, and only the Cr and C precipitated.
An XRD was used to determine the phase compositions and to probe the diffusion of W into Cr_3C_2. The XRD-patterns of the E20 and E10 powders and coatings in the as-sprayed and the heat-treated states are presented in fig. 6.17. Moreover, the pattern of the reference coating, designated as Cr_3C_2-NiCr ref., displays diffraction peak 2θ locations for the W-depleted binder and Cr_3C_2 phases. The region-of-interest in fig. 6.17 is limited to 2θ=38-45°, which contains the (111) peak of the Ni-binder together with the (112) and (203) peaks of Cr_3C_2. The $(W_{1-x}Cr_x)_2C$ phase, commonly found in Cr_3C_2-WC-Ni systems, e.g. in 73WC-20Cr_3C_2-7Ni coatings [21, 22], should appear at 2θ=41-41.5° [90]. However, the XRD-pattern shows no peaks in this range, which corresponds with the results presented by refs. [58, 107, 109].
The W-content dependent lattice parameters for $(Cr_{1-x}W_x)_3C_2$ grains have been reported by Stecher et al. [90]. Based on these lattice parameters, the W content of $x = 0.04$ in $(Cr_{1-x}W_x)_3C_2$ was determined in both E20 and E10 feedstock powders. Moreover, a slightly elevated W content, $x = 0.06$, in $(Cr_{1-x}W_x)_3C_2$ was calculated for both as-sprayed coatings. Thus, additional W was diffused into the primary carbides during the intense heating of the powder during spraying. As expected, the heat-treatment at 800 °C resulted in even further diffusion of W into the primary carbides; the W contents in the $(Cr_{1-x}W_x)_3C_2$ grains in the heat-treated E20 and E10 coatings were $x = 0.08$ and $x = 0.07$, respectively. The calculation of the W content in the Ni-binder by the shift of the (111) Ni-peak is challenging due to the excess Cr in the lattice. However, the Ni (111) peaks of the E20 and E10 have shifted towards lower 2θ angles (i.e. towards the left) than the W-depleted Ni (111) of the plain Cr_3C_2-NiCr reference coating. This indicates the presence of W in the binder phase of both E20 and E10. The pronounced peak shifting is especially noticeable in the heat-treated E20 and E10 coatings, which illustrates the excess amount of W remaining in the binder after the heat-treatment.
The impact of W on the mechanical properties of the binder was probed by performing nanoindentation matrices on the cross-sections of the heat-treated K2-C2 and E20 coatings. In this case, K2-C2 was chosen as a reference Cr_3C_2-NiCr coating because the

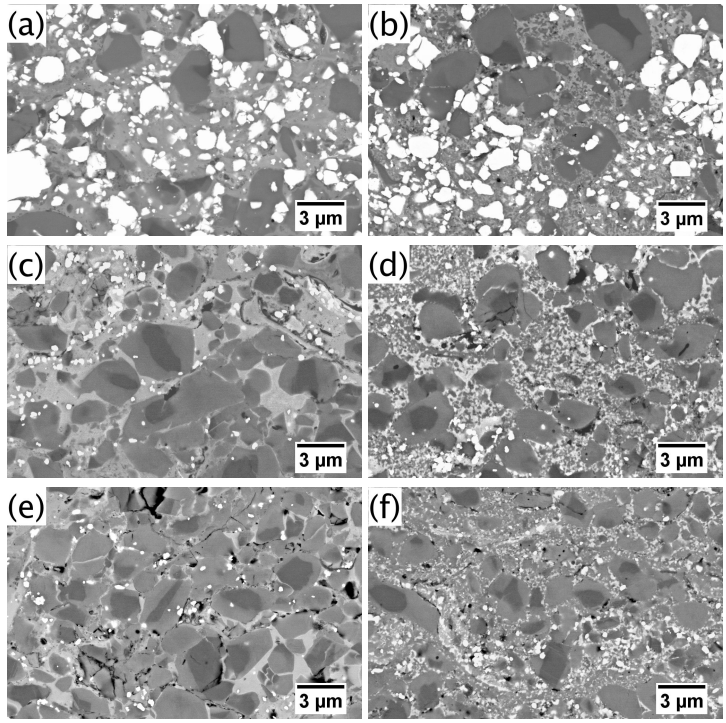

Figure 6.16: BSE-micrographs of as-sprayed (left column) and heat-treated at 800 °C for 8 h (right column) K2-W1 (a,b), E20 (c,d), and E10 (e,f) coatings [Publication IV].

primary carbide size and the carbide volume fraction after heat-treatment corresponded most closely to the heat-treated E20 coating. Fig. 6.18 presents the hardness frequency histograms of 650 indents on the heat-treated K2-C2 and E20 coatings. The K2-C2 coating shows bi-modal distribution, which is typical for two-phase composite materials [132]. The hardness of the binder and the carbide phases are in the range of 6-16 GPa and 18-26 GPa, respectively. The hardness frequency histogram of the E20 coating, however, does not display a similarly pronounced bi-modal distribution. This was attributed to the substitutional W in the binder phase of the E20 coating, because W is known to be a strong solid solution strengthener in the Ni-lattice [142]. While residual W possibly improved the hardness of the binder in E20, the W alloying of the carbide phase shows no significant increase in hardness. Previously it has been claimed that W increases the hardness of Cr_7C_3 solely at elevated testing temperatures [94].

6.3.3 Wear resistance of the coatings

Fig. 6.19 (a) presents the room temperature abrasion resistances of the K2-W1, K2-C2, E20, and E10 coatings in their as-sprayed and heat-treated states. The K2-C2 coating, which represents a commercially available Cr_3C_2-NiCr composition, shows the highest wear rate in the as-sprayed state. The influence that a modest 2 vol.% addition of WC has on abrasion resistance is demonstrated by comparing the wear rates of the as-sprayed K2-C2 and E20 coatings. Even though the binder content in both as-sprayed coatings was comparable, roughly 40 vol.%, the wear rate of E20 is markedly lower than it is in K2-C2.

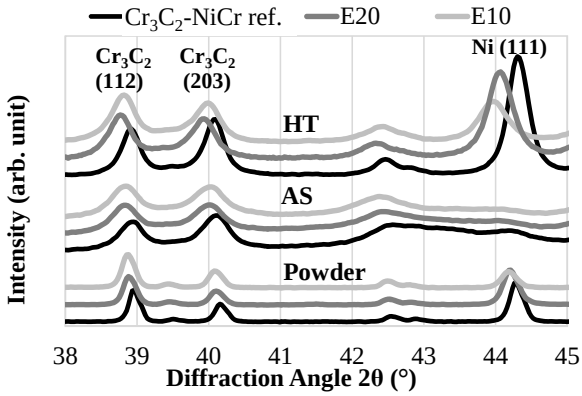

Figure 6.17: XRD patterns of E20 and E10 powders, as-sprayed, and heat-treated (8h/800 °C) coatings. The Cr_3C_2-NiCr ref. shows the W free Cr_3C_2 and Ni-binder diffraction peaks [Publication IV].

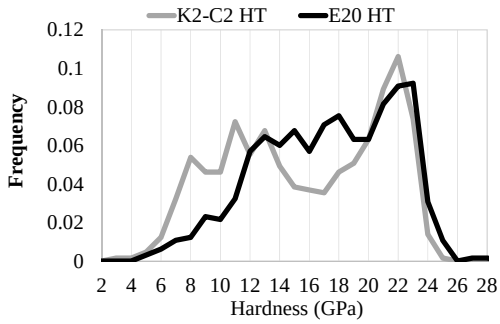

Figure 6.18: Frequency diagrams of grid indentations of heat-treated (8h/800 °C) K2-C2 and E20 coatings illustrating the presumed solid solution strengthening of the binder in E20 by W [Publication IV].

The higher content of Cr_3C_2 grains in the E10 coating yielded only a moderate decrease in the wear rate. Moreover, as-sprayed K2-W1, which contained the highest proportion of WC (20 vol.%) displays almost corresponding wear rates to E20 and E10. Thus, the highest WC content does not yield superior abrasion resistance at room temperature.
The microstructural changes and improvements in the high-stress abrasion resistance of Cr_3C_2-NiCr coatings resulting from the heat-treatment were discussed previously in Sections 6.1 and 6.2. Here, similar improvements in high-stress abrasion resistance are visible in all of the studied coatings. Even though the microstructure in E10 displays cracks and the carbides are poorly embedded in the binder, in its heat-treated state the coating shows remarkable abrasion resistance. In fact, the heat-treatment reduced the wear rate by a factor of 4. This is owing to the ability of the heat-treated binder to absorb vast amounts of mechanical energy. Possibly, in E10 the heat-induced changes in the binder are so clearly manifested in the abrasion resistance because of its low binder content.
The abrasion resistance of metal matrix composites at high temperatures is governed by the mechanical properties of the binder, the carbides, and the abrasive particles. Furthermore, the total carbide content, the oxidation resistance of the material, and the

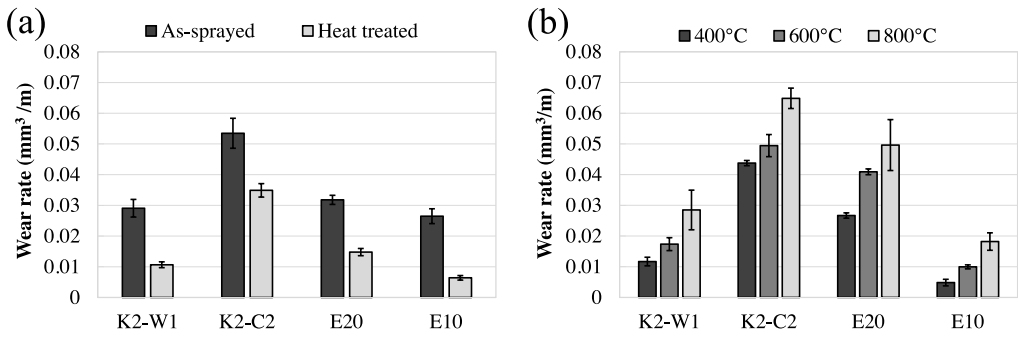

Figure 6.19: Wear rates of K2-W1, K2-C2, E20, and E10 coatings tested at room temperature (a) and at elevated temperatures (400, 600 and 800 °C) (b) [Publication IV].

development of a protective mechanically-mixed layer from the abrasive debris can also have a major influence on the wear properties of the material [83, 117].
Fig. 6.19 (b) shows the high-temperature abrasion resistances at 400, 600 and 800 °C of heat-treated (8h/ 800 °C) coatings. As stated before, the dislocation migration promoted by thermal activation reduced the yield stress of the material, which resulted in increased wear rates at elevated testing temperatures [139]. The plain Cr_3C_2-NiCr coating K2-C2 has the highest wear rate, while the E10 has the lowest. However, the difference between K2-C2 and E20 is not as clearly manifested at elevated temperatures as it was at room temperature. At 800 °C, the W still pins the migrating dislocation and hardens the Ni-lattice, though not as efficiently as it does at room temperature [142]. Therefore, although the influence of additional WC on the wear rate is noticeable at 800 °C, it is not so prominent as at lower temperatures.
Furthermore, the K2-W1 coating displays distinctly lower wear rates at 800 °C than the E20. Given the higher hot-hardness of WC over Cr_3C_2 [83], the relatively coarse WC grains in K2-W1 can be more beneficial at elevated temperatures than at room temperature. In addition, there is a significant difference in the wear rates of E20 and E10 at 800 °C. Similar results were presented in ref. [143], wherein a higher Cr_3C_2 content resulted in a marked increase in erosion resistance at 600 °C. Therefore, the high carbide content is beneficial at elevated service temperatures. Clearly, neither the relatively high as-sprayed porosity or the partially inadequate embedding of the carbides in the binder inhibit the abrasion resistance of E10 at elevated temperatures. The dense and smeared surface layer in the wear track of E10 suggests that thermo-mechanical treatment of loaded abrasives densified the tribolayer of the coating during high-temperature abrasion [Publication IV].

6.3.4 Conclusions

The 10 wt.% WC alloying of Cr_3C_2-Ni coatings resulted in a microstructure consisting of core-rim structured Cr_3C_2-$(Cr,W)_3C_2$ grains and a Ni-binder with excess W. As with commercially available 75Cr_3C_2-25NiCr coatings, during heat-treatment the fine chromium carbides precipitated in the supersaturated binder phase. However, the W remained in the binder and thus appeared to provide solid solution hardening in the Ni-lattice. The improvement in technical performance caused by WC alloying was clearly demonstrated in the abrasion tests. The Cr_3C_2-WC-Ni coatings have improved abrasion resistance at room and elevated temperatures when compared with the commercially

available 75Cr_3C_2-25NiCr. The wear testing, however, took only 5 minutes. Therefore, the oxidation of WC did not play a major role in wear resistance. In the future also prolonged wear and oxidation tests should be applied to these coatings, in order to probe the service characteristics over a long time.

6.4 Characteristics of the Laser Post-Treated Cr_3C_2-WC-Ni Coatings

The historically relevant 70WC-24Cr_3C_2-6Ni composition is not usually regarded as a simple binary carbide hardmetal, as it typically contains three carbides: WC, Cr_3C_2, and $(W_{1-x}Cr_x)_2C$ [21, 22]. Even though this composition has been commercially available for over 50 years, the properties and formation conditions of $(W_{1-x}Cr_x)_2C$ in Ni-binder are yet to be extensively studied. Interestingly, the binary carbide compositions studied in Section 6.3 showed no formation of $(W_{1-x}Cr_x)_2C$ during the feedstock powder preparation, the deposition of the coating, or during the heat-treatment at 800 °C.
Due to the appropriate residual carbide-forming elements (Cr, W, and C), the binder of the as-sprayed 45Cr_3C_2-37WC-NiCoCr coating is considered chemically suitable for the precipitation of Cr-rich $(W_{1-x}Cr_x)_2C$ grains. However, the challenge is to reach a sufficiently high temperature without remelting the coating. This is where the aforementioned laser post-treatment is utilized, i.e. it focuses enough thermal input accurately on the coated layer and thus precipitates $(W_{1-x}Cr_x)_2C$.

6.4.1 Structure and properties of the coatings

The BSE-images of the microstructures of the as-sprayed, heat-treated and laser post-treated coatings are shown in fig. 6.20. The corresponding as-sprayed and heat-treated coatings were presented previously in fig. 6.16. The as-sprayed coating in (a) shows a C, Cr, and W-supersaturated binder, which is reflected in the wide distribution of the gray-scale values. In furnace heat-treated coatings, however, only chromium carbides precipitated, which are seen as dark entities in the binder in (b). The microstructures of the laser post-treated coatings, see (c) and (d), show the precipitation of a phase with intermediate gray-scale values. Thus, the 20.8 J/mm^2 fluence treated coating in particular, which is characterized by the most pronounced laser-induced microstructural changes, shows a distinct trimodal distribution of the gray-scale values. The chemistry of the phase with intermediate gray-scale values was studied with EDX point analysis. The locations for EDX-spots and corresponding at.% compositions are shown in table 6.1. The EDX-analysis indicates that the chemistry of Spot 3 corresponds to Cr-rich $(W_{1-x}Cr_x)_2C$ grains.
The XRD patterns of the as-sprayed and the post-treated coatings over 2θ = 38-46° are shown in fig. 6.21. In the as-sprayed coatings, the wide amorphous peak over 2θ = 43-45° demonstrates the supersaturated binder phase. The furnace and laser post-treatments resulted in crystallization and grain growth in the metallic binder phase, which is reflected in the form of the narrow binder peaks in the post-treated coatings. The most significant impact of the laser post-treatment is the formation of the $(W_{1-x}Cr_x)_2C$ precipitates. This is shown by the rise of the (101) peak of the hexagonal W_2C above 2θ = 41°. The intensity of the peak is increased with the applied laser fluence. These precipitates show a Cr content of x = 0.6-0.7, which is determined by the composition-dependent lattice parameters of Stecher et al. [90]. The x = 0.6-0.7 in $(W_{1-x}Cr_x)_2C$ also corresponds to the EDX-analysis presented in table 6.1. Furthermore, the consumption of W from the

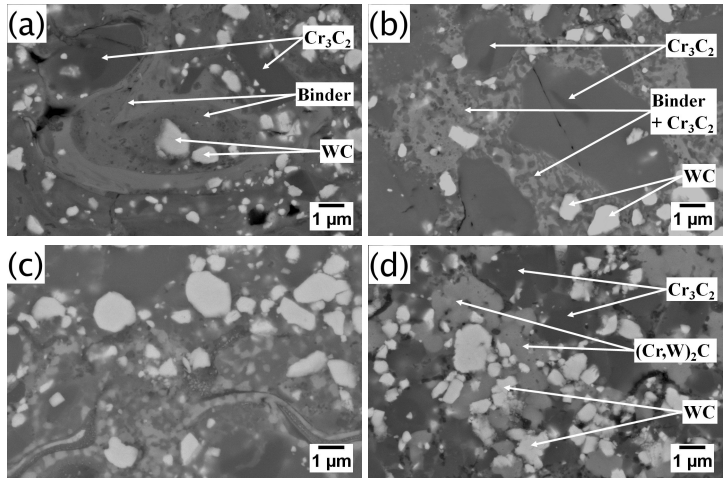

Figure 6.20: BSE-micrographs of the as-sprayed (a), heat-treated (8h/800 °C) (b) and laser post-treated coatings with fluences of 15.6 J/mm^2 (c), and 20.8 J/mm^2 (d). Micrographs were taken 20μm below the surface [Publication V].

Table 6.1: The EDX-analysis of the Spots 1-4, shown in the BSE-micrograph of the 20.8 J/mm^2 laser-treated coating. The spot compositions are presented in at.% [Publication V].

Spot	W	Cr	C	Ni	Co
Spot 1	-	63	37	-	-
Spot 2	3	57	36	1	1
Spot 3	19	45	31	3	1
Spot 4	43	3	53	-	3

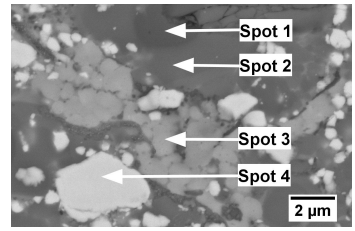

binder during laser treatment is demonstrated by the shift of the binder peaks in the laser-treated coatings towards higher scattering angles. As was also shown previously in Section 6.3, the furnace heat-treatment at 800 °C does not yield precipitation of the $(W_{1-x}Cr_x)_2C$ carbide.

The grid indentation technique was used to probe the hardness of the $(W_{1-x}Cr_x)_2C$ precipitates. Fig. 6.22 displays the nanohardness frequency diagram of the furnace heat-treated and the 20.8 J/mm^2 fluence laser post-treated coatings. The most pronounced difference between these two samples occurs in the hardness range of 18-26 GPa. The frequency difference between furnace heat-treated and laser post-treated coating in this hardness range manifests the mechanical properties of $(W_{1-x}Cr_x)_2C$ precipitates. The hardness of $(W_{1-x}Cr_x)_2C$ is comparable with the prismatic plane hardness in WC.

6.4.2 Wear resistance of the coatings

The high-stress abrasion resistances of the as-sprayed, the furnace heat-treated, and the laser post-treated coatings are presented in fig. 6.23. As expected, the conventional heat-treatment in the furnace made the brittle binder phase more ductile, which is

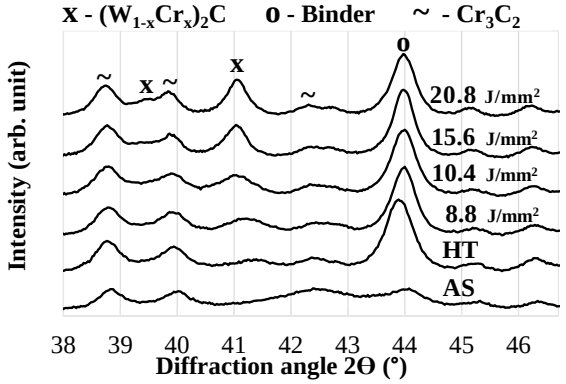

Figure 6.21: XRD patterns of as-sprayed (AS), furnace heat-treated (8h/800 °C) (HT), and laser post-treated coatings [Publication V].

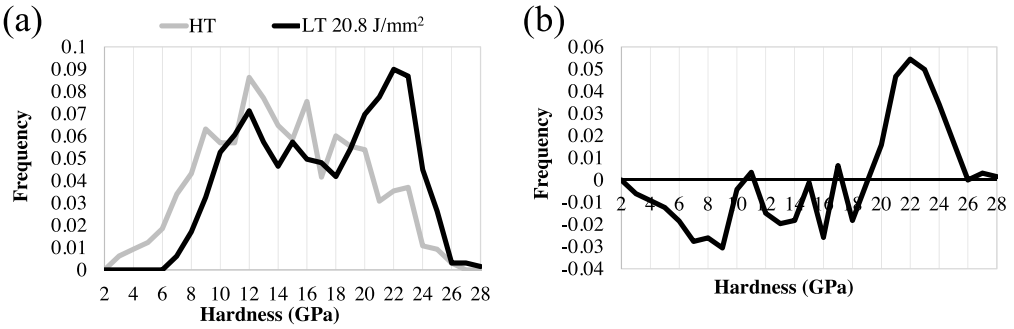

Figure 6.22: Nanohardness presented in frequency diagrams (a) of coatings after furnace heat-treatment (8h/800 °C) (HT) and 20.8 J/mm^2 laser fluence treatment (LT) and (b) the difference between them [Publication V].

illustrated by the superior abrasion resistance of the heat-treated coating over the as-sprayed coating. Moreover, the laser post-treated coatings display even higher wear resistance. This is probably due to the high proportion of $(W_{1-x}Cr_x)_2C$ precipitates. Interestingly, the 20.8 J/mm^2 laser fluence-treated coating shows a wear rate close to the industrial WC-CoCr benchmark. This illustrates the attractive technical performance of the $(W_{1-x}Cr_x)_2C$ grains in thermally sprayed coatings.
The $(W_{1-x}Cr_x)_2C$ grains were characterized after the abrasion test by SEM-analysis of the wear track. Figure 6.24 shows the SE and BSE images of the wear track of the 20.8 J/mm^2 fluence treated coating. The figure shows cracked primary Cr_3C_2 grains and a crack-free $(W_{1-x}Cr_x)_2C$ agglomerate. This indicates that the Cr-rich $(W_{1-x}Cr_x)_2C$ has preferable mechanical properties to Cr_3C_2. Obviously, the mechanical properties, such as the ductility of these carbides, would need more systematic studies in the future.

6.4.3 Surface inspection

The surface inspection of the coating after laser post-treatment is presented in fig. 6.25. The post-treatment induced cracking is clearly visible in the dye-penetrant and white

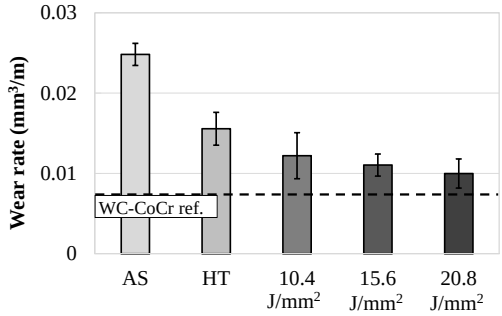

Figure 6.23: High-stress abrasion wear rates of as-sprayed (AS), furnace heat-treated (HT), and laser post-treated coatings tested at room temperature [Publication V].

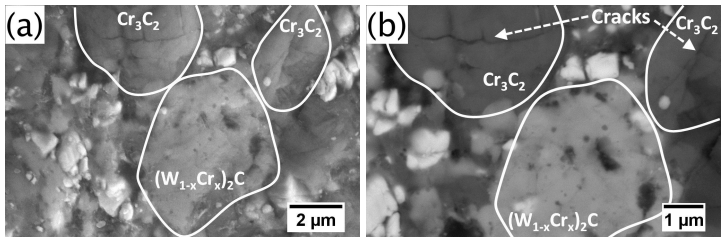

Figure 6.24: SE (a) and BSE (b) micrographs of the high-stress abrasion wear track of the laser post-treated (20.8 J/mm^2) coating displaying the cracking of the primary Cr_3C_2 grains [Publication V].

developer soaked surfaces at the bottom of the figure. The furnace-treated coating (HT) demonstrates the challenges of using the conventional heat-treatment procedure for HVOF coatings. Due to the CTE differences between the coating and the substrate, the coating cracks and may subsequently spall off from the substrate. The laser-treated coatings, however, display similar cracks to the ones presented with the plain Cr_3C_2-NiCr. The propagation of these cracks was attributed to the steep temperature gradients which occur during laser processing. The most wear-resistant coating, laser-treated with a low traveling speed at 20.8 J/mm^2 fluence, has a particularly crack-free surface. Thus, the corrosion protection capacity of this post-treated coating is considered to be comparable to the as-sprayed coating.

6.4.4 Conclusions

The influence of the previously-introduced laser post-treatment on the HVOF sprayed $45Cr_3C_2$-37WC-18Ni coating was studied. With the laser fluencies that were used, no melting of the deposit was detected. The microstructure of the post-treated coatings consisted of primary Cr_3C_2 and WC carbides together with Cr-rich $(W_{1-x}Cr_x)_2C$ precipitates. Moreover, the size of the precipitated $(W_{1-x}Cr_x)_2C$ grains increased with higher laser fluencies. The hardness of $(W_{1-x}Cr_x)_2C$ was within the range of the prismatic plane in the WC grains. Furthermore, the SEM inspection of the abraded surface indicated a somewhat ductile character of the $(W_{1-x}Cr_x)_2C$ precipitates. Therefore, the abrasion resistance of the coating treated with the 20.8 J/mm^2 laser fluence corresponded

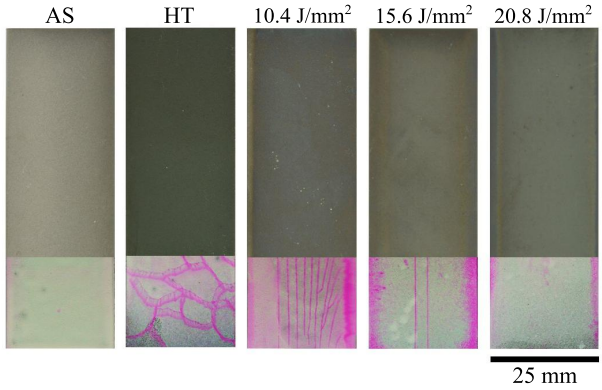

Figure 6.25: The surface inspection of the as-sprayed (AS), furnace heat-treated (HT), and laser post-treated surfaces. Overlaid photographs of the dye-penetrant treated surface (bottom) display post-treatment induced cracking [Publication V].

closely to the industrial HVOF sprayed WC-CoCr benchmark coating. The potential of laser-treated $45Cr_3C_2$-37WC-Ni coatings for high-temperature service is dependent on the high-temperature oxidation resistance of the $(W_{1-x}Cr_x)_2C$ precipitates. Therefore, in the future, the oxidation properties of $(W_{1-x}Cr_x)_2C$ grains should be studied with various Cr contents (e.g. $x = 0.2$ - 0.8) at temperatures above 600 °C.

7 Conclusions

Industrially deployed thermally-sprayed abrasion-resistant coatings for high service temperatures typically comprise Cr_3C_2 hardphases in a Ni-binder. In this work, the technical performance, i.e. abrasion resistance, of these coatings was probed at room and elevated testing temperatures. This has led to suggestions for enhancing the abrasion resistance by post-treatments and alloying. From a technical perspective, both alloying and post-treatments were considered as potential candidates to increase the service life of the coatings in harsh conditions. However, the economic incentive to utilise these abrasion improvement methods depends heavily on the future costs of industrial laser equipment and tungsten carbide.

7.1 Scientific Contribution

The research questions, presented in Chapter 1, are addressed below.

I Cr_3C_2-NiCr Coatings

1. **What roles do the feedstock powder consolidation method (sintering vs. plasma-densification) and the spray process (gas-fueled HVOF, liquid-fueled HVOF, and HVAF) method play in the microstructure of the 75Cr_3C_2-25NiCr coating?**

   The powder consolidation method had a distinct influence on the microstructure of as-sprayed coatings; both the carbide size and the carbide size-distribution of the coating stemmed from the feedstock powder microstructure. Furthermore, the plasma-densified feedstock powder yielded minimal decarburization and dense coating.
   Dissolution of Cr_3C_2 carbides into the Ni-binder was strongly affected by the selection of the spray process. The ethene-fueled HVOF torch led to the most pronounced dissolution of the carbides into the binder phase. In contrast, the coatings deposited by the HVAF torch displayed the lowest degree of carbide dissolution. The carbide loss in HVOF sprayed coatings appeared mostly through carbide dissolution. In HVAF coatings, however, the dominant carbide loss mechanism was selective carbide rebounding. This selective carbide rebounding was reduced when plasma-densified feedstock powders were used.
   However, prolonged aging at 800 °C transformed the microstructure towards its thermodynamic equilibrium, i.e the Ostwald ripening of the microstructure resulted in

coatings with coarse coalescent carbides. Therefore, the carbide size in the feedstock powder and the degree of carbide dissolution during spraying had only minimal influence on the microstructure of the coating after the long service at high temperatures.

2. **How does the microstructure of the coating influence the abrasion protection capacity of thermally sprayed Cr_3C_2-NiCr coatings at room and elevated temperatures?**

   The room temperature abrasion resistance of Cr_3C_2-NiCr coating was governed by the carbide dissolution induced supersaturated and brittle binder. The wear tracks of the brittle as-sprayed binder displayed cracking and the detachment of large chunks of material. The ethene-fueled HVOF-deposited coating, in particular, demonstrated brittle behavior during abrasion tests at room temperature, while the HVAF torch produced coatings displayed higher resistance against wear. Therefore, the room temperature abrasion resistance in the coatings sprayed by these processes was in the decreasing order of M3-HVAF, K2-HVOF, and DJ-HVOF.
   After heat-treatment, however, the brittleness of the supersaturated binder was neutralized by the precipitation of the chromium carbides. Therefore, the heat treatment greatly enhanced the abrasion resistance of the Cr_3C_2-NiCr coatings. The most pronounced increase in the abrasion resistance took place in coatings with the highest degree of carbide dissolution, i.e. in HVOF coatings. In HVAF sprayed coatings, wherein the carbide loss was dominated by selective carbide rebounding, the heat-treatment induced improvement in abrasion resistance was almost negligible. Thus, the deposition process resulted in only slight differences in the abrasion resistance of the heat-treated Cr_3C_2-NiCr coatings.
   The major contributors to the high-temperature abrasion resistance of the Cr_3C_2-NiCr coatings can be divided into metallurgical reactions and heat-induced changes in the mechanical properties. The metallurgical reactions in the Cr_3C_2-NiCr microstructure included precipitation of carbides, grain growth of the metallic Ni-binder, and eventually the Ostwald ripening. The onset of precipitation greatly increased the ductility of the binder and thus improved the high-stress abrasion resistance of the coating at room temperature. However, during high-temperature service, the thermal activation induced dislocation migration, which softened the binder metal to such an extent that the high-stress abrasion resistance was reduced. Therefore, the coating, which showed brittle behavior and microcracking during the room temperature abrasion, displayed a ductile appearance and a smeared wear surface after the abrasion at elevated temperatures.
   The material loss by abrasion at 800 °C was only slightly higher than that of the as-sprayed coatings at room temperature. This demonstrated the suitability of Cr_3C_2-NiCr coatings for high-temperature service. Due to the equalization of the as-sprayed microstructures at high temperatures, for coatings intended for elevated temperatures the spray economics (e.g. price of consumables and deposition efficiency) appear to play the most important role when considering the choice of feedstock powder and spray process.

II Laser treated Cr_3C_2-NiCr coatings

3. **Can the high-stress abrasion resistance of Cr_3C_2-NiCr coating be improved by laser-induced nanosized chromium carbide precipitation?**

   In the laser post-treatment experiments performed with low laser fluences, the subsurface zone of the coating displayed small precipitates. The size of these precipitates was within the range at which the particle hardening was considered as an active binder-strengthening mechanism. The high-stress abrasion tests demonstrated that this rapid post-treatment improved the abrasion resistance significantly. However, the fast laser spot velocity yielded steep temperature gradients in the coatings, which was manifested in the propagation of vertical cracks running along the laser scanning direction. These cracks can reduce the corrosion-protection capacity of the coating. Therefore, further process optimization is required to *cure* the supersaturated and brittle as-sprayed binder without promoting cracks in the coating.

III WC alloyed Cr_3C_2-Ni

4. **How do the interactions between the WC and Cr_3C_2 grains influence the microstructure and mechanical properties in 10 wt.% WC-alloyed Cr_3C_2 based coatings?**

   The addition of WC in the Cr_3C_2-based composition resulted in the formation of core-rim structured $(Cr,W)_3C_2-Cr_3C_2$ grains and W containing binder. Another chemically possible phase, $(W_{1-x},Cr_x)_2C$, did not precipitate in the binder during spraying or heat-treatment.
   The most important contribution of WC addition to the mechanical properties was detected after the heat-treatment, as the W presumably increased the hardness of the binder by substitutional solid solution hardening. However, no significant differences in nanohardness were detected between $(Cr,W)_3C_2$ and plain Cr_3C_2 grains at room temperature.

5. **What is the contribution of the 10 wt.% WC addition to the abrasion resistance of the Cr_3C_2-based coatings?**

   The influence of the WC alloying was demonstrated by comparing the experimental $70Cr_3C_2$-10WC-20Ni coating against the commercially available $75Cr_3C_2$-25NiCr coating. The experimental $70Cr_3C_2$-10WC-20Ni coating demonstrated superior abrasion resistance to the plain Cr_3C_2-NiCr coatings both at room and elevated testing temperatures. The W in the binder, which presumably strengthened the binder via substitutional solid solution hardening, was considered to be one of the factors contributing to such a clear improvement in the abrasion resistance.
   The abrasion resistance of $70Cr_3C_2$-10WC-20Ni was at a comparable level with the commercially available $45Cr_3C_2$-37WC-Ni composition at room temperature, yet slightly inferior at elevated temperatures. The superior abrasion resistance of $45Cr_3C_2$-37WC-Ni over $70Cr_3C_2$-10WC-20Ni in an elevated temperature was

attributed to the high hot-hardness of the coarse WC grains.

6. **What is the significance of the metallic binder content in the abrasion resistance of the WC-alloyed Cr_3C_2-rich coatings?**

   The experimental coating with low binder content, designated as $80Cr_3C_2$-10WC-10Ni, presented superior abrasion resistance at both room and elevated testing temperatures. The improved abrasion resistance was attributed to the high carbide content and the W strengthened Ni-binder. Even though the as-sprayed $80Cr_3C_2$-10WC-10Ni coating had cracks and relatively high porosity, during high-temperature abrasion the surface was densified by the thermo-mechanical work induced through the loaded abrasive particles. The high abrasion resistance of the $80Cr_3C_2$-10WC-10Ni composition at 800 °C makes it an attractive wear-protection solution for high-temperature applications. However, the high-temperature oxidation of these experimental compositions should be probed prior to industrial pilot-scale studies.

IV Laser treated Cr_3C_2-WC-Ni coatings

7. **Is it possible to precipitate the $(W_{1-x}Cr_x)_2C$ phase in the binder of the as-sprayed binary carbide Cr_3C_2-WC-Ni coatings by laser post-treatment without remelting the coating?**

   The binder phase of as-sprayed $45Cr_3C_2$-37WC-Ni coating contained the residual carbide-forming elements W, Cr, and C due to the spraying-induced dissolution and decomposition of the carbides. As with the Cr_3C_2-NiCr coatings, during heat-treatment at 800 °C only chromium carbides precipitated and thus the residual W remained in the binder. The high-fluence laser treatment, which heated the binder in the subsurface zone nearly to its melting point, resulted in the formation of coarse $(W_{1-x}Cr_x)_2C$ precipitates. Therefore, the cross-section of the coating displayed a gradient structure in which the vast majority of the $(W_{1-x}Cr_x)_2C$ precipitates were found in the area close to the surface of the coating. In the treatment parameters suitable for the most pronounced $(W_{1-x}Cr_x)_2C$ precipitation, the high fluence was achieved by a slow 6 mm/s laser traveling velocity from which no cracking of the coating was detected.

8. **Do Cr-rich $(W_{1-x}Cr_x)_2C$ precipitates improve the abrasion resistance of the coating?**

   In the nanohardness tests, the effect of the $(W_{1-x}Cr_x)_2C$ precipitates were clearly visible in the frequency diagram. The hardness was in the same range as in the prismatic plane in WC grains. Moreover, the abrasion resistance of the laser post-treated coating with the $(W_{1-x}Cr_x)_2C$ grains was far superior to the abrasion resistances of the as-sprayed or furnace heat-treated coatings. Thus, the improved wear resistance induced by the laser post-treatment was mainly attributed to these $(W_{1-x}Cr_x)_2C$ precipitates. Furthermore, in the SEM-images of the abraded surfaces, the $(W_{1-x}Cr_x)_2C$ displayed no cracking. This indicated that the ductility of the $(W_{1-x}Cr_x)_2C$ grains is higher than that of the Cr_3C_2 grains.

7.2 Suggestions for the Future Work

Because the microstructure in Cr_3C_2-NiCr coating is susceptible to heat-induced changes, the heat-treatment prior to high-temperature wear testing plays an important role in simulating service at elevated temperatures. In this work, the longest heat-treatment duration prior to the abrasion tests was 100 h. In the future, the high-temperature abrasion resistance should be probed after even more prolonged heat-treatments (>1000 h), when the microstructure presents an interconnected network of coarse carbides.
The experimental 70Cr_3C_2-10WC-20Ni and 80Cr_3C_2-10WC-10Ni coatings demonstrated high abrasion resistances at room and elevated temperatures. However, the technical performance at high temperatures is also largely influenced by the oxidation resistance of the coatings and their sensitivity to cracking due to the CTE mismatch between the coating and the substrate. Thus, in order to deploy the experimental coatings in industry, the emphasis in future studies should be placed on the high-temperature oxidation characteristics and thermal cracking resistance of these coating compositions.
The laser post-treated coatings, as long as the coating was kept in a solid state, displayed technical potential as an effective method for increasing the coatings' abrasion resistance. However, the economic viability for using this type of post-treatment procedure in industry relies heavily on the future price development of the laser equipment. The other kinds of post-treatment methods, such as carefully optimized induction heating, could cut down the required investment costs and thus reduce the costs of the post-treatment procedure. More specific applications in which the laser post-treated coatings could be utilized should be searched for together with an industrial partner.

Bibliography

[1] J.H. Tylczak. Abrasive wear. In *ASM Handbook Volume 18*, pages 184 – 190. ASM International, 1992.

[2] M.A. Moore and F.S. King. Abrasive wear of brittle solids. *Wear*, 60(1):123 – 140, 1980. doi: 10.1016/0043-1648(80)90253-7.

[3] K. Schröter. Verfahren zur Herstellung einer harten Schmelzlegierung fuer Arbeitswerkzeuge, insbesondere Ziehsteine. (DE 498349 C), May 1930.

[4] H.M. Ortner, P. Ettmayer, and Kolaska H. The history of the technological progress of hardmetals. *International Journal of Refractory Metals and Hard Materials*, 44: 148 – 159, 2014. doi: 10.1016/j.ijrmhm.2013.07.014.

[5] L Prakash. Fundamentals and General Applications of Hardmetals. In V. K. Sarin, D. Mari, L. Llanes, and C. Nebel, editors, *Comprehensive Hard Materials*, pages 29 – 90. Elsevier, 2014.

[6] R. Kieffer and P. Schwarzkopf. *Hartstoffe und Hartmetalle*. Springer-Verlag Wien, 1. edition, 1953. doi: 10.1007/978-3-7091-3901-1.

[7] M.U. Schoop. Über die Herstellung von Überzügen aus Wolfram, bzw. Wolfram-Karbid mittels der "Schoop-Pistole". *Korrosion und Metallschutz*, 18:243 – 244, 1942.

[8] H.B. Poorman, R. Sargent and L Headlee. Method and apparatus utilizing detonation waves for spraying and other purposes. (US 2714563 A), August 1955.

[9] Y. A. Kharlamov. Bonding of detonation-sprayed coatings. *Thin Solid Films*, 54 (3):271 – 278, 1978. doi: 10.1016/0040-6090(78)90383-8.

[10] P. Vuoristo. 4.10 - Thermal Spray Coating Processes. In S. Hashmi, G. F. Batalha, C. J. Tyne, and B. Yilbas, editors, *Comprehensive Materials Processing*, pages 229 – 276. Elsevier, 2014. doi: https://doi.org/10.1016/B978-0-08-096532-1.00407-6.

[11] L.-M. Berger. Coatings by Thermal Spray. In V. K. Sarin, D. Mari, L. Llanes, and C. Nebel, editors, *Comprehensive Hard Materials*, pages 471 – 506. Elsevier, 2014.

[12] F. Goodwin, K.U. Guruswamy, S.and Kainer, C Kammer, W Knabl, A Koethe, Leichtfried G., Schlamp G., R. Stickler, and H. Warlimont. 3.1 - Metals. In W Martienssen and H. Warlimont, editors, *Handbook of Condensed Matter and Materials Data*, pages 161 – 422. Springer, 2005.

[13] H. Warlimont. 3.2 - Ceramics. In W Martienssen and H. Warlimont, editors, *Handbook of Condensed Matter and Materials Data*, pages 431 – 476. Springer, 2005.

[14] M. Uusitalo, R. Backman, L.-M. Berger, Vuoristo P., and T. A. Mäntylä. Oxidation resistance of carbides in chlorine-containing atmospheres. *High Temperature Materials and Processes*, 21(5):307–320, 2002. doi: 10.1515/HTMP.2002.21.5.307.

[15] R. Silberglitt, J. T. Bartis, B. G. Chow, D. L. An, and K. Brady. Tungsten: Case Example of a Critical Raw Material. In *Critical Materials: Present Danger to U.S. Manufacturing*, pages 167–173, Santa Monica, California, 2013. RAND Corporation.

[16] S. Norgren, J. García, A. Blomqvist, and L. Yin. Trends in the P/M hard metal industry. *International Journal of Refractory Metals and Hard Materials*, 48:31–45, 2015. doi: 10.1016/j.ijrmhm.2014.07.007.

[17] European Commission. Communication from the Commission to the European Parliament, The Council, The European Economic and Social Committee and the Committee of the Regions on the 2017 list of Critical Raw Materials for the EU. 2017.

[18] J.M. Koffskey and J.F. Pelton. Process of flame spraying a tungsten carbide-chromium carbide-nickel coating, and article produced thereby. (US 3071489 A), January 1963.

[19] J.F. Pelton and J.M. Koffskey. Coating composition, method of application, and product thereof. (US 3150938 A), September 1964.

[20] G.-L. Hou, H.D. Zhou, Y.-L. An, G. Liu, J.-M. Chen, and J. Chen. Microstructure and high-temperature friction and wear behavior of WC-$(W,Cr)_2C$-Ni coating prepared by high velocity oxy-fuel spraying. *Surface and Coatings Technology*, 206 (1):82–94, 2011. doi: 10.1016/j.surfcoat.2011.06.047.

[21] L.-M. Berger, S. Saaro, T. Naumann, M. Kašparova, and F. Zahálka. Influence of feedstock powder characteristics and spray processes on microstructure and properties of WC–$(W,Cr)_2C$–Ni hardmetal coatings. *Surface and Coatings Technology*, 205(4):1080–1087, 2010. doi: 10.1016/j.surfcoat.2010.07.032.

[22] G. Bolelli, L.-M. Berger, M. Bonetti, and L. Lusvarghi. Comparative study of the dry sliding wear behaviour of HVOF-sprayed WC–$(W,Cr)_2C$–Ni and WC–CoCr hardmetal coatings. *Wear*, 309(1–2):96–111, 2014. doi: 10.1016/j.wear.2013.11.001.

[23] M. Kašparová, F. Zahálka, and S. Houdková. WC-Co and Cr_3C_2-NiCr Coatings in Low- and High-Stress Abrasive Conditions. *Journal of Thermal Spray Technology*, 20(3):412–424, 2011. doi: 10.1007/s11666-010-9523-y.

[24] L.-M. Berger. Binary WC- and Cr_3C_2-containing hardmetal compositions for thermally sprayed coatings. *IOP Conference Series: Materials Science and Engineering*, 118:012010, 2016. doi: 10.1088/1757-899X/118/1/012010.

[25] J. K. N. Murthy, K. Satya Prasad, K. Gopinath, and B. Venkataraman. Characterisation of HVOF sprayed Cr_3C_2-50(Ni20Cr) coating and the influence of binder properties on solid particle erosion behaviour. *Surface and Coatings Technology*, 204(24):3975–3985, 2010. doi: 10.1016/j.surfcoat.2010.04.069.

[26] J. M. Guilemany, J. M. Miguel, S. Vizcaino, C. Lorenzana, J Delgado, and J Sanchez. Role of heat treatments in the improvement of the sliding wear properties of Cr_3C_2–NiCr coatings. *Surface and Coatings Technology*, 157(2):207–213, 2002. doi: 10.1016/S0257-8972(02)00148-2.

[27] S. Zimmermann and H. Kreye. Chromium carbide coatings produced with various HVOF spray systems. In *Proceedings of the 9. National Thermal Spray Conference*, pages 147–152, Cincinnati, OH, Oct. 1996. ASM International.

[28] S. Matthews, M. Hyland, and B. James. Microhardness variation in relation to carbide development in heat treated Cr_3C_2–NiCr thermal spray coatings. *Acta Materialia*, 51(14):4267–4277, 2003. doi: 10.1016/S1359-6454(03)00254-4.

[29] S. Matthews, B. James, and M. Hyland. The role of microstructure in the mechanism of high velocity erosion of Cr_3C_2–NiCr thermal spray coatings: Part 2 — Heat treated coatings. *Surface and Coatings Technology*, 203(8):1094–1100, 2009. doi: 10.1016/j.surfcoat.2008.10.013.

[30] S. Matthews and L.-M. Berger. Long-term compositional/microstructural development of Cr_3C_2-NiCr coatings at 500 °C, 700 °C and 900 °C. *International Journal of Refractory Metals and Hard Materialsy*, 59:1–18, 2016. doi: 10.1016/j.ijrmhm.2016.05.010.

[31] L. Zhong and X. Ma. Recent Developments in High Power Semiconductor Diode Lasers. In P. Predeep, editor, *Optoelectronics - Devices and Applications*, pages 325–348. InTech, 2011.

[32] J. Mateos, J. M. Cuetos, E. Fernández, and R. Vijande. Tribological behaviour of plasma-sprayed WC coatings with and without laser remelting. *Wear*, 239:274–281, 2000. doi: 10.1016/S0043-1648(00)00325-2.

[33] P. Serra, J. M. Miguel, J. L. Morenza, and J.M. Guilemany. Structural characterization of laser-treated Cr_3C_2–NiCr coatings. *Journal of Materials Research*, 16 (12):3416–3422, 2001. doi: 10.1557/JMR.2001.0470.

[34] J. Morimoto, Y. Sasaki, S. Fukuhara, N. Abe, and M. Tukamoto. Surface modification of Cr_3C_2–NiCr cermet coatings by direct diode laser. *Vacuum*, 80(11–12): 1400–1405, 2006. doi: 10.1016/j.vacuum.2006.01.070.

[35] H. Chen, C. Xu, Q. Zhou, I. M. Hutchings, P. H. Shipway, and J. Liu. Micro-scale abrasive wear behaviour of HVOF sprayed and laser-remelted conventional and nanostructured WC-Co coatings. *Wear*, 258(1–4):333–338, 2005. doi: 10.1016/j.wear.2004.09.044.

[36] T. Kuwashima, I. Takahashi, T. Tomita, and A. Ohmori. The Effect of Simultaneous Laser Irradiation on a Cr_3C_2-Ni-Cr Coating Produced by the High-Velocity Oxy-Fuel Spraying Process. *Materials Transactions*, 45(6):1864–1868, 2004. doi: 10.2320/matertrans.45.1864.

[37] B. S. Mann, V. Arya, and B. K. Pant. High-Power Diode Laser Surface Treated HVOF Coating to Combat High Energy Particle Impact Wear. *Journal of Materials Engineering and Performance*, 22(7):1995–2004, 2013. doi: 10.1007/s11665-013-0475-5.

[38] M. Rakhes, E. Koroleva, and Z. Liu. Improvement of corrosion performance of HVOF MMC coatings by laser surface treatment. *Surface Engineering*, 27(10): 729 – 733, 2011. doi: 10.1179/1743294411Y.0000000001.

[39] E. Chikarakara, S. Aqida, D. Brabazon, S. Naher, J. A. Picas, M. Punset, and A. Forn. Surface modification of HVOF thermal sprayed WC-CoCr coatings by laser treatment. *International Journal of Material Forming*, 3(1):801 – 804, 2010. doi: 10.1007/s12289-010-0891-0.

[40] S. H. Zhang, J. H. Yoon, M. X. Li, T. Y. Cho, Y. K. Joo, and J. Y. Cho. Influence of CO2 laser heat treatment on surface properties, electrochemical and tribological performance of HVOF sprayed WC-24%Cr_3C_2-6%Ni coating. *Materials Chemistry and Physics*, 119(3):458 – 464, 2010. doi: 10.1016/j.matchemphys.2009.09.025.

[41] S. H. Zhang, T. Y. Cho, J. H. Yoon, M. X. Li, P. W. Shum, and S. C. Kwon. Investigation on microstructure, surface properties and anti-wear performance of HVOF sprayed WC-CrC-Ni coatings modified by laser heat treatment. *Materials Science and Engineering B: Solid-State Materials for Advanced Technology*, 162(2): 127 – 134, 2009. doi: 10.1016/j.mseb.2009.03.017.

[42] M. Varga, H. Winkelmann, and E. Badisch. Impact of microstructure on high temperature wear resistance. *Procedia Engineering*, 10:1291 – 1296, 2011. doi: 10.1016/j.proeng.2011.04.215.

[43] M. Varga. High temperature abrasive wear of metallic materials. *Wear*, 376 – 377: 443 – 451, 2017. doi: 10.1016/j.wear.2016.12.042.

[44] F. Otsubo, H. Era, K. Kishitake, and T. Uchida. Properties of Cr_3C_2-NiCr cermet coating sprayed by high power plasma and high velocity oxy-fuel processes. *Journal of Thermal Spray Technology*, 9(4):499 – 504, 2000. doi: 10.1007/BF02608553.

[45] C.-J. Li, G.-C. Ji, Y.-Y. Wang, and K. Sonoya. Dominant effect of carbide rebounding on the carbon loss during high velocity oxy-fuel spraying of Cr_3C_2 – NiCr. *Thin Solid Films*, 419(1 – 2):137 – 143, 2002. doi: 10.1016/S0040-6090(02)00708-3.

[46] G.-C. Ji, C.-J. Li, Y.-Y. Wang, and W.-Y. Li. Microstructural characterization and abrasive wear performance of HVOF sprayed Cr_3C_2-NiCr coating. *Surface and Coatings Technology*, 200(24):6749 – 6757, 2006. doi: 10.1016/j.surfcoat.2005.10.005.

[47] S. Siegmann and C. Abert. 100 years of thermal spray: About the inventor Max Ulrich Schoop. *Surface and Coatings Technology*, 220:3 – 13, 2013. doi: 10.1016/j.surfcoat.2012.10.034.

[48] L. Pawlowski. *The Science and Engineering of Thermal Spray Coatings*. John Wiley and Sons, Ltd, 2. edition, 2008.

[49] M. Oksa, E. Turunen, T. Suhonen, T. Varis, and S.-P. Hannula. Optimization and Characterization of High Velocity Oxy-fuel Sprayed Coatings: Techniques, Materials, and Applications. *Coatings*, 1:17 – 52, 2011. doi: 10.1088/1757-899X/118/1/012010.

[50] J.A. Browning. Flame spray method and apparatus. (US 4634611A), January 1987.

[51] M.L. Thorpe and Richter H.J. A pragmatic analysis and comparison of HVOF processes. *Journal of Thermal Spray Technology*, 1(2):161 – 170, 1992. doi: 10.1007/BF02659017.

[52] R. Kaufold, A.J. Rotolico, J. Nerz, and B. Kushner. Deposition of Coatings Using a New High Velocity Combustion Spray Gun. In *NTSC Proceedings*, pages 561 – 569, Materials Park, Ohio, 1990. ASM international.

[53] H. Kreye and S. Schwetzke, S. Zimmermann. High Velocity Oxy-Fuel Flame Spraying-Process and Coating Characteristics. In *Proceedings of the 9. National Thermal Spray Conference*, pages 451 – 456, Cincinnati, OH, Oct. 1996. ASM International.

[54] K. Sakaki and Shimizu Y. Effect of the increase in the entrance convergent section length of the gun nozzle on the high-velocity oxygen fuel and cold spray process. *Journal of Thermal Spray Technology*, 10(3):487 – – 496, 2001. doi: 10.1361/1059963017.

[55] V.V. Sobolev, J.M. Guilemany, and J. Nutting. *High Velocity Oxy Fuel Spraying: Theory, Structure-property Relationships and Applications*. Maney Publishing, 1. edition, 2004.

[56] H. Kreye, F. Gärtner, A. Kirsten, and R. Schwetzke. High Velocity Oxy-Fuel Flame Spraying State of the Art, Prospects and Alternatives. In *5th Colloquim "High Velocity Oxy Fuel Spraying"*, pages 5 – 18, Erding, Germany, 2000. GTS.

[57] V. Matikainen, G. Bolelli, H. Koivuluoto, M. Honkanen, M. Vippola, L. Lusvarghi, and P. Vuoristo. A Study of Cr_3C_2-Based HVOF- and HVAF-Sprayed Coatings: Microstructure and Carbide Retention. *Journal of Thermal Spray Technology*, 26 (6):1239 – 1256, 2017. doi: 10.1007/s11666-017-0578-x.

[58] V. Matikainen, G. Bolelli, H. Koivuluoto, P. Sassatelli, L. Lusvarghi, and P. Vuoristo. Sliding wear behaviour of HVOF and HVAF sprayed Cr_3C_2-based coatings. *Wear*, 2017. doi: 10.1016/j.wear.2017.04.001.

[59] G. Bolelli, L.-M. Berger, T. Börner, H. Koivuluoto, V. Matikainen, L. Lusvarghi, N. Lyphout, N. Markocsan, P. Nylén, P. Sassatelli, R. Trache, and P Vuoristo. Sliding and abrasive wear behaviour of HVOF- and HVAF-sprayed Cr_3C_2 – NiCr hardmetal coatings. *Wear*, 358 – 359:32 – 50, 2016. doi: 10.1016/j.wear.2016.03.034.

[60] L.-M. Berger, R. Puschmann, J. Spatzier, and S. Matthews. Potential of HVAF Spray Processes. *Thermal Spray Bulletin*, 1:16 – 20, 2013.

[61] J. Jacobs, M.M. Hyland, and M. De Bonte. Comparative study of WC-cermet coatings sprayed via the HVOF and the HVAF Process. *Journal of Thermal Spray Technology*, 7(2):213 – 218, 1998. doi: 10.1361/105996398770350954.

[62] G. Bolelli, L.-M. Berger, T. Börner, H. Koivuluoto, L. Lusvarghi, C. Lyphout, N. Markocsan, V. Matikainen, P. Nylén, P. Sassatelli, R. Trache, and P. Vuoristo. Tribology of HVOF- and HVAF-sprayed WC – 10Co4Cr hardmetal coatings: A comparative assessment. *Surface and Coatings Technology*, 265:125 – 144, 2015. doi: 10.1016/j.surfcoat.2015.01.048.

[63] A Verstak and V. Baranovski. AC-HVAF Sprayed Tungsten Carbide: Properties and Application. In *Thermal Spray 2006: Building on 100 Years of Success*, pages 643 – 648, Seattle, Washington, 2006. ASM International.

[64] V.E. Baranovski and A.V. Baranovski. Supersonic material flame spray method and apparatus. (US 20110229649A1), September 2011.

[65] L.P. Fauchais, J.V.R. Heberlein, and M. Boulos. *Thermal Spray Fundamentals*. Springer US, 1. edition, 2014. doi: 10.1007/978-0-387-68991-3.

[66] M.P. Planche, B Normand, H. Liao, G. Rannou, and C. Coddet. Influence of HVOF spraying parameters on in-flight characteristics of Inconel 718 particles and correlation with the electrochemical behaviour of the coating. *Surface and Coatings Technology*, 157(2–3):247–256, 2002. doi: 10.1016/S0257-8972(02)00158-5.

[67] K. Korpiola, J.P. Hirvonen, L. Laas, and F. Rossi. The Influence of Nozzle Design on HVOF Exit Gas Velocity and Coating Microstructure. *Journal of Thermal Spray Technology*, 6(4):469–474, 1997. doi: 10.1007/s11666-997-0033-51.

[68] K. Korpiola, H. Jalkanen, J.P. Hirvonen, L. Laas, and F. Rossi. Oxygen partial pressuremeasurement in the HVOF gun tail flame. In *Proceedings of the 8th National Thermal Spray Conference*, pages 181–648, Houston, USA, 1995. ASM International.

[69] V. Katranidis, S. Gu, T.R. Reina, E. Alpay, B. Allcock, and S. Kamnis. Experimental study of high velocity oxy-fuel sprayed WC-17Co coatings applied on complex geometries. Part B: Influence of kinematic spray parameters on microstructure, phase composition and decarburization of the coatings. *Surface and Coatings Technology*, 328:499–512, 2017. doi: 10.1016/j.surfcoat.2017.09.027.

[70] C. Verdon, S. Karimi, and J.-L. Martin. A study of high velocity oxy-fuel thermally sprayed tungsten carbide based coatings. Part 1: Microstructures. *Materials Science and Engineering: A*, 246(1-2):11–24, 1998. doi: 10.1016/S0921-5093(97)00759-4.

[71] W. Trompetter, M. Hyland, D. McGrouther, P. Munroe, and A. Markwitz. Effect of substrate hardness on splat morphology in high-velocity thermal spray coatings. *Journal of Thermal Spray Technology*, 15(4):663–669, 2006. doi: 10.1361/105996306X147261.

[72] S. Kuroda, Y. Tashiro, H. Yumoto, S. Taira, H. Fukanuma, and S. Tobe. Peening action and residual stresses in high-velocity oxygen fuel thermal spraying of 316L stainless steel. *Journal of Thermal Spray Technology*, 10(2):367–374, 2001. doi: 10.1361/105996301770349457.

[73] H.O. Pierson. *Handbook of Refractory Carbides and Nitride*. William Andrew Publishing, 1. edition, 1996. doi: 10.1016/B978-081551392-6.50004-0.

[74] W. Lengauer. Chapter 7: Transition Metal Carbides, Nitrides, and Carbonitrides. In R Riedel, editor, *Handbook of Ceramic Hard Materials*, pages 202–252. WILEY-VCH Verlag GmbH, 2000. doi: 10.1002/9783527618217.ch7.

[75] M. Venkatraman and J.P. Neumann. The C-Cr (Carbon-Chromium) System. *Bulletin of Alloy Phase Diagrams*, 11(2):152––159, 1990. doi: 10.1007/BF02841701.

[76] A.S. Kurlov and A.I. Gusev. Tungsten carbides and W-C phase diagram. *Inorganic Materials*, 42(2):121––127, 2006. doi: 10.1134/S0020168506020051.

[77] A.S. Kurlov and A.I. Gusev. *Tungsten Carbides Structure, Properties and Application in Hardmetals*. Springer International Publishing, 1. edition, 2013. doi: 10.1007/978-3-319-00524-9.

[78] L. Pons. Plastic properties in tungsten monocarbide. In *Proceedings of an international symposium of anisotropy in single-crystal refractory compounds*, pages 393 – 333. Plenum press, June. 1968.

[79] J.D. Bolton and M. Redington. Plastic deformation mechanisms in tungsten carbides. *Journal of Materials Science*, 15(12):3150 – 3156, 1980. doi: 10.1007/BF00550388.

[80] J. Yuan, Q. Zhan, J. Huang, S. Ding, and H. Li. Decarburization mechanisms of WC-Co during thermal spraying: Insights from controlled carbon loss and microstructure characterization. *Materials Chemistry and Physics*, 142(1):165 – 171, 2013. doi: 10.1016/j.matchemphys.2013.06.052.

[81] K. Günther, J. Liefeith, P. Henckell, Y. Ali, and J.P. Bergmann. Influence of processing conditions on the degradation kinetics of fused tungsten carbides in hardfacin. *International Journal of Refractory Metals & Hard Materials*, 70:224 – 231, 2018. doi: 10.1016/j.ijrmhm.2017.10.015.

[82] H. Taimatsu, S. Sugiyama, and Y. Kodaira. Synthesis of W_2C by Reactive Hot Pressing and Its Mechanical Properties. *Materials Transactions*, 49(6):1256 – 1261, 2008. doi: 10.2320/matertrans.MRA2007304.

[83] H. Berns and S. Koch. High temperature sliding abrasion of a nickel-base alloy and composite. *Wear*, 225 – 229:154 – 162, 1999. doi: 10.1016/S0043-1648(99)00008-3.

[84] L.-M. Berger, P. Vuoristo, T. Mäntylä, and W. Gruner. A study of oxidation behaviour of WC-Co, Cr_3C_2-NiCr and TiC-Ni-based materials in thermal spray processes. In *Proceedings of the 15th International Thermal Spray Conference*, pages 75 – 82, Nice, France, 1998. ASM International.

[85] M. Venkatraman and J.P. Neumann. The C-Cr (Carbon-Chromium) System. *Bulletin of Alloy Phase Diagrams*, 11(2):152 – 159, 1990. doi: 10.1007/BF02841701.

[86] Mayr W., W. Lengauer, P. Ettmayer, D. Rafaja, J. Baue, and M. Bohr. Phase equilibria and multiphase reaction diffusion in the Cr-C and Cr-N systems. *Journal of Phase Equilibria*, 20(1):35 – 44, 1999. doi: 10.1361/105497199770335929.

[87] V.E. Buchanan, D.G. McCartney, and P.H. Shipwaya. A comparison of the abrasive wear behaviour of iron-chromium based hardfaced coatings deposited by SMAW and electric arc spraying. *Wear*, 264(7-8):542 – 549, 2008. doi: 10.1016/j.wear.2007.04.008.

[88] J. Feng, B. Xiao, R. Zhou, Y.H. Jiang, and Q.H. Cen. Calculation and simulation for the mechanical properties of carbides and borides in cast iron. *Procedia Engineering*, 31:676 – 681, 2012. doi: 10.1016/j.proeng.2012.01.1085.

[89] A. Westegren. Complex Chromium and Iron Carbides. *Nature*, 132:480, 1933. doi: 10.1038/132480a0.

[90] P. Stecher, F. Benesovsky, and H. Nowotny. Investigation for the Chromium-Tungsten-Carbon system. In *Planseeberichte für pulvermetallurgie 12*, pages 89 – 95, Reutte, Austria, 1964. Plansee Group.

[91] E. Rudy and Y. A. Chang. In *Plansee Proceedings 1964*, pages 786 – 822, Reutte, Austria, 1965. Plansee Group.

[92] M. Brieseck, M. Bohn, and W. Lengauer. Diffusion and solubility of Cr in WC. *Journal of Alloys and Compounds*, 489(2):408 – 414, 2010. doi: 10.1016/j.jallcom.2009.09.137.

[93] Z. Tükör, W. D. Schubert, A. Bicherl, A. Bock, and B. Zeiler. Formation of W-Cr-Phases During the Production of Cr-doped WC Powders. In *17th Plansee Seminar*, pages HM 44/1 – HM 44/10, Reutte, Austria, 2009. Plansee Group.

[94] K. Yamamoto, S. Inthidech, N. Sasaguri, and Y. Matsubara. Influence of Mo and W on High Temperature Hardness of Cr_7C_3 Carbide in High Chromium White Cast Iron. *Materials Transactions*, 55(4):684 – 689, 2014. doi: 10.2320/matertrans.F-M2014801.

[95] A. Watson and A. Kroupa. Carbon – Chromium – Tungsten. In G. Effenberg and S. Ilyenko, editors, *Landolt-Börnstein - Group IV Physical Chemistry 11E2*, pages 379 – 396. SpringerMaterials, 2010. doi: 10.1007/978-3-642-02700-0_25.

[96] S. Matthews and B. James. Review of thermal spray coating applications in the steel industry: Part 1—hardware in steel making to the continuous annealing process. *Journal of Thermal Spray Technology*, 19(6):1267 – –1276, 2010. doi: 10.1007/s11666-010-9518-8.

[97] A. Vardelle, C. Moreau, J. Akedo, et al. The 2016 Thermal Spray Roadmap. *Journal of Thermal Spray Technology*, 25(8):1376 – 1440, 2016. doi: 10.1007/s11666-016-0473-x.

[98] T.Y. Velikanova, A.A. Bondar, and A.V. Grytsiv. The chromium-nickel-carbon (Cr-Ni-C) phase diagram. *Journal of Phase Equilibria*, 20(2):676 – 681, 1999. doi: 10.1007/s11669-999-0011-3.

[99] K. Natesan and T. F. Kassner. Thermodynamics of carbon in nickel, iron-nickel and iron-chromium-nickel alloys. *Metallurgical Transactions*, 4(11):2557 – 2566, 1973. doi: 10.1007/BF02644258.

[100] T. Varis, T. Suhonen, O. Calonius, J. Čuban, and M. Pietola. Optimization of HVOF Cr_3C_2-NiCr coating for increased fatigue performance. *Surface and Coatings Technology*, 305:123 – 131, 2016. doi: 10.1016/j.surfcoat.2016.08.012.

[101] J.D. Reardon, R. Mignogna, and F.N. Longo. Plasma- and vacuum-plasma-sprayed Cr_3C_2 composite coatings. *Thin Solid Films*, 83(3):345 – 351, 1981. doi: 10.1016/0040-6090(81)90637-4.

[102] D. L. Houck and R.F. Cheney. Comparison of properties of Cr_3C_2-Ni-Cr coatings thermally sprayed from pre-alloyed and mechanically mixed powders. *Thin Solid Films*, 118(4):507 – 513, 1984. doi: 10.1016/0040-6090(84)90279-7.

[103] J.M. Guilemany, J. Nutting, and N. Llorcalsern. Microstructural examination of HVOF chromium carbide coatings for high-temperature applications. *Journal of Thermal Spray Technology*, 5(4):483 – 489, 1996. doi: 10.1007/BF02645280.

[104] L.-M. Berger, S. Saaro, T. Naumann, M. Kašparová, and F. Zahálka. Microstructure and Properties of HVOF-Sprayed WC-$(W,Cr)_2C$-Ni Coatings. *Journal of Thermal Spray Technology*, 17(3):395 – 403, 2008. doi: 10.1007/s11666-008-9189-x.

[105] H. Henke, D. Adam, A. Köhler, and Heimann R.B. Development and testing of HVOF-sprayed tungsten carbide coatings applied to moulds for concrete roof tiles. *Wear*, 256:81 – 87, 2004. doi: 10.1016/S0043-1648(03)00348-X.

[106] H.M. Hawthorne, B. Arsenault, J.P. Immarigeon, J.G. Legoux, and V.R. Parameswaran. Comparison of slurry and dry erosion behaviour of some HVOF thermal sprayed coatings. *Wear*, 225 – 229(2):825 – 834, 1999. doi: 10.1016/S0043-1648(99)00034-4.

[107] W. Zhou, K. Zhou, Y Li, C Deng, and K. Zeng. High temperature wear performance of HVOF-sprayed Cr_3C_2-WC-NiCoCrMo and Cr_3C_2-NiCr hardmetal coatings. *Applied Surface Science*, 416:33 – 44, 2017. doi: 10.1016/j.apsusc.2017.04.132.

[108] W. Zhou, K. Zhou, C Deng, K. Zeng, and Y Li. Hot corrosion behavior of HVOF-sprayed Cr_3C_2-WC-NiCoCrMo coating. *Ceramics International*, 2017. doi: 10.1016/j.ceramint.2017.04.109.

[109] I. Hulka, V.A. Şerban, I. Secoşan, P. Vuoristo, and K. Niemi. Wear properties of CrC – 37WC – 18M coatings deposited by HVOF and HVAF spraying processes. *Surface and Coatings Technology*, 210:15 – 20, 2012. doi: 10.1016/j.surfcoat.2012.07.077.

[110] Zum Gahr K.-H. Wear by hard particles. *Tribology International*, 31(10):587 – 596, 1998. doi: 10.1016/S0301-679X(98)00079-6.

[111] K. Kato. Wear mode transitions. *Scripta Metallurgica et Materialia*, 25(5):815 – 820, 1990. doi: 10.1016/0956-716X(90)90118-Z.

[112] Y. Wang and S.M. Hsu. Wear and wear transition mechanisms of ceramics. *Wear*, 195(1-2):112 – 122, 1996. doi: 10.1016/0043-1648(95)06800-7.

[113] J.D. Gates. Two-body and three-body abrasion: A critical discussion. *Wear*, 214 (1):139 – 146, 1998. doi: 10.1016/S0043-1648(97)00188-9.

[114] M. Varga, L. Widder, M. Griesinger, K. Adam, and E. Badisch. Wear progress and mechanisms in high temperature sieves. *Engineering Failure Analysis*, 61:46 – 53, 2016. doi: 10.1016/j.engfailanal.2015.07.032.

[115] J. Larsen-Basse and B. Premaratne. Effect of relative hardness on transitions in abrasive wear mechanisms . In *Proceedings of the 4th International Conference on Wear of Materials*, pages 161 – 166, USA, 1983. ASME.

[116] H. Berns and A. Fischer. Tribological stability of metallic materials at elevated temperatures. *Wear*, 162 – 164:441 – 449, 1993. doi: 10.1016/0043-1648(93)90528-T.

[117] H. Berns and S.D. Franco. Effect of coarse hard particles on high-temperature sliding abrasion of new metal matrix composites. *Wear*, 203 – -204:608 – 614, 1997. doi: 10.1016/S0043-1648(96)07427-3.

[118] H. Winkelmann, E. Badisch, M Varga, and H. Danninger. Wear Mechanisms at High Temperatures. Part 3: Changes of the Wear Mechanism in the Continuous Impact Abrasion Test with Increasing Testing Temperature. *Tribology Letters*, 384- – 385:114 – 123, 2010. doi: 10.1007/s11249-009-9534-3.

[119] M. Varga and E. Badisch. Temperature and load influence on in-situ formed layers during high temperature abrasion. *Wear*, 384-–385:114–123, 2017. doi: 10.1016/j.wear.2017.04.020.

[120] A.J. Gant, M.G. Gee, and B. Roebuck. Rotating wheel abrasion of WC/Co hardmetals. *Wear*, 258(1–4):55–68, 2005. doi: 10.1016/j.wear.2004.09.028.

[121] R.J.K. Wood. Tribology of thermal sprayed WC–Co coatings. *International Journal of Refractory Metals and Hard Materials*, 28(1):82–94, 2010. doi: 10.1016/j.ijrmhm .2009.07.011.

[122] S. Houdková, F. Zahálka, M. Kašparová, and L.-M. Berger. Comparative Study of Thermally Sprayed Coatings Under Different Types of Wear Conditions for Hard Chromium Replacement. *Tribology Letters*, 43(2):139–154, 2011. doi: 10.1007/ s11249-011-9791-9.

[123] N. Vashishtha and S.G. Sapate. Abrasive wear maps for High Velocity Oxy Fuel (HVOF) sprayed WC-12Co and Cr_3C_2-25NiCr coatings . *Tribology International*, 114:290–305, 2017. doi: 10.1016/j.triboint.2017.04.037.

[124] N. Vashishtha, S.G. Sapate, P. Bagde, and A.B. Rathod. Effect of heat treatment on friction and abrasive wear behaviour of WC-12Co and Cr_3C_2-25NiCr coatings. *Tribology International*, 118:381–399, 2018. doi: 10.1016/j.triboint.2017.10.017.

[125] N. Vashishtha and S.G. Khatirkar, R.K. Sapate. Tribological behaviour of HVOF sprayed WC-12Co, WC-10Co-4Cr and Cr_3C_2-25NiCr coatings. *Tribology International*, 105:55–68, 2017. doi: 10.1016/j.triboint.2016.09.025.

[126] J.K.N. Murthy and B. Venkataraman. Abrasive wear behaviour of WC–CoCr and Cr_3C_2–20(NiCr) deposited by HVOF and detonation spray processes. *Surface and Coatings Technology*, 200(8):55–68, 2006. doi: 10.1016/j.triboint.2016.09.025.

[127] B.Q. Wang and L. Luer. High temperature erosion of Cr_3C_2–NiCr thermal spray coatings — The role of phase microstructure. *Wear*, 174(1–2):177–185, 1994. doi: 10.1016/0043-1648(94)90100-7.

[128] S. Matthews, B. James, and M. Hyland. Erosion of oxide scales formed on Cr_3C_2–NiCr thermal spray coatings. *Corrosion Science*, 50(11):3087–3094, 2008. doi: 10.1016/j.corsci.2008.08.032.

[129] S. Matthews, B. James, and M. Hyland. High temperature erosion of Cr_3C_2–NiCr thermal spray coatings — The role of phase microstructure. *Surface and Coatings Technology*, 203(9):1144–1153, 2009. doi: 10.1016/j.surfcoat.2008.10.008.

[130] L.-M. Berger, R. Trache, F.-L. Toma, S. Thiele, J. Norpoth, and L. Janka. Development of cost-effective hardmetal coating solutions for high-temperature applications Part one: Feedstock powders, cost-effectiness and coating properties. *Thermal Spray Bulletin*, 8(2):126–135, 2015.

[131] W.C. Oliver and G.M. Pharr. An improved technique for determining hardness and elastic modulus using load and displacement sensing indentation experiments. *Journal of Materials Research*, 7(6):1564–1583, 1992. doi: 10.1557/JMR.1992.1564.

[132] G. Constantinides, K.S. Ravi Chandran, F.-J. Ulm, and K.J. Van Vliet. Grid indentation analysis of composite microstructure and mechanics: Principles and validation. *Material Science and Engineering: A*, 430(1–2):189–202, 2006. doi: 10.1016/j.msea.2006.05.125.

[133] N.X. Randall, M. Vandamme, and F.-J. Ulm. Nanoindentation analysis as a two-dimensional tool for mapping the mechanical properties of complex surfaces. *Journal of Materials Research*, 24(3):679–690, 2009. doi: 10.1557/jmr.2009.0149.

[134] Š. Houdková, O. Bláhová, F. Zahálka, and M. Kašparová. The Instrumented Indentation Study of HVOF-Sprayed Hardmetal Coatings. *Journal of Thermal Spray Technology*, 21(1):77–85, 2012. doi: 10.1007/s11666-011-9677-2.

[135] V. Katranidis, S. Gu, B. Allcock, and S. Kamnis. Experimental study of high velocity oxy-fuel sprayed WC-17Co coatings applied on complex geometries. Part A: Influence of kinematic spray parameters on thickness, porosity, residual stresses and microhardness. *Surface and Coatings Technology*, 311:206–215, 2017. doi: 10.1016/j.surfcoat.2017.01.015.

[136] R. K. Kumar, M. Kamaraj, S. Seetharamu, T. Pramod, and P. Sampathkumaran. Effect of Spray Particle Velocity on Cavitation Erosion Resistance Characteristics of HVOF and HVAF Processed 86WC-10Co4Cr Hydro Turbine Coatings. *Journal of Thermal Spray Technology*, 25(6):1217––1230, 2016. doi: 10.1007/s11666-016-0427-3.

[137] J. K. N. Murthy, S. Bysakh, K. Gopinath, and B. Venkataraman. Microstructure dependent erosion in Cr_3C_2–20(NiCr) coating deposited by a detonation gun. *Surface and Coatings Technology*, 202(1):1–12, 2007. doi: 10.1016/j.surfcoat.2007.03.017.

[138] K. Hokkirigawa and K. Kato. An experimental and theoretical investigation of ploughing, cutting and wedge formation during abrasive wear. *Tribology International*, 21(1):51–57, 1988. doi: 10.1016/0301-679X(88)90128-4.

[139] E. Rabinowicz. *Friction and Wear of Materials*. John Wiley & Sons, 2. edition, 1995.

[140] P. Haasen. *Physical Metallurgy*. Cambridge University Press, 1. edition, 1978. pp. 341–342.

[141] P. Chivavibul, M. Watanabe, S. Kuroda, and K. Shinoda. Effects of carbide size and Co content on the microstructure and mechanical properties of HVOF-sprayed WC–Co coatings. *Surface and Coatings Technology*, 202(3):509–521, 2007. doi: 10.1016/j.surfcoat.2007.06.026.

[142] H. Rehman. *Solid Solution Strengthening and Diffusion in Nickel- and Cobalt-based Superalloys*. PhD thesis, Friedrich-Alexander-Universität, 2016.

[143] I. Hussainova and M. Antonov. Elevated temperature wear of chromium carbide cermets. *Proceedings of the Estonian Academy of Sciences*, 4(9):261–271, 2003.

Publications

Publication I

L. Janka, J. Norpoth, R. Trache, S. Thiele, and L.-M.Berger, "HVOF- and HVAF-Sprayed Cr_3C_2-NiCr Coatings Deposited from Feedstock Powders of Spherical Morphology: Microstructure Formation and High-Stress Abrasive Wear Resistance Up to 800 °C", *Journal of Thermal Spray Technology* vol 98, No. 7 pp. 1720-–1731, Oct. 2017.

The original publication is available at DOI: 10.1007/s11666-017-0621-y

Publication II

L. Janka, J. Norpoth, R. Trache, and L.-M. Berger, "Influence of heat treatment on the abrasive wear resistance of a Cr_3C_2-NiCr coating deposited by an ethene-fuelled HVOF spray process", *Surface & Coatings Technology*, vol 291, pp. 444–451, Apr. 2016.

Publication III

L. Janka, J. Norpoth, S. Eicher, M. Rodríguez Ripoll, and P. Vuoristo, "Improving the toughness of thermally sprayed Cr_3C_2-NiCr hardmetal coatings by laser post-treatment", *Materials and Design*, vol 98, pp. 135 – 142, May 2016.

Publication IV

L. Janka, L.-M. Berger, J. Norpoth, C. Tomastik, V. Matikainen, and P. Vuoristo, "Improving the high temperature abrasion resistance of thermally sprayed Cr_3C_2-NiCr coatings by WC addition", *Surface & Coatings Technology*, vol 337, pp. 296 – 305, March 2018.

Publication V

L. Janka, J. Norpoth, C. Tomastik, V. Matikainen, and P. Vuoristo, "Laser-induced precipitation of $(W_{1-x}Cr_x)_2C$: Mixed carbide phase for improved wear resistance of thermally sprayed hardmetal coatings", *Surface & Coatings Technology*, vol 337, pp.177–185, March 2018.

Tampereen teknillinen yliopisto
PL 527
33101 Tampere

Tampere University of Technology
P.O.B. 527
FI-33101 Tampere, Finland

ISBN 978-952-15-4271-8
ISSN 1459-2045